İSTANBUL TECHNICAL UNIVERSITY ★ GRADUATE SCHOOL OF SCIENCE ENGINEERING AND TECHNOLOGY

INVESTIGATION OF THE TURNING PERFORMANCE OF A SURFACE COMBATANT WITH URANS

M.Sc. THESIS

Süleyman DUMAN

Department of Naval Architecture and Marine Engineering

Naval Architecture and Marine Engineering Programme

JUNE 2016

İSTANBUL TECHNICAL UNIVERSITY ★ GRADUATE SCHOOL OF SCIENCE ENGINEERING AND TECHNOLOGY

INVESTIGATION OF THE TURNING PERFORMANCE OF A SURFACE COMBATANT WITH URANS

M.Sc. THESIS

Süleyman DUMAN
(508141014)

Department of Naval Architecture and Marine Engineering

Naval Architecture and Marine Engineering Programme

Thesis Advisor: Prof. Dr. Şakir BAL

JUNE 2016

İSTANBUL TEKNİK ÜNİVERSİTESİ ★ FEN BİLİMLERİ ENSTİTÜSÜ

BİR SU ÜSTÜ SAVAŞ GEMİSİNİN DÖNME PERFORMANSININ URANS KULLANILARAK İNCELENMESİ

YÜKSEK LİSANS TEZİ

Süleyman DUMAN
(508141014)

Gemi İnşaatı ve Gemi Makineleri Mühendisliği Anabilim Dalı

Gemi İnşaatı ve Gemi Makineleri Mühendisliği Programı

Tez Danışmanı: Prof. Dr. Şakir BAL

HAZİRAN 2016

Süleyman DUMAN, a **M.Sc.** student of İTU **Graduate School of Science Engineering and Technology** student ID **508141014**, successfully defended the **thesis** entitled **"Investigation of the Turning Performance of a Surface Combatant with URANS"**, which he prepared after fulfilling the requirements specified in the associated legislations, before the jury whose signatures are below.

Thesis Advisor :	**Prof. Dr. Şakir BAL** İstanbul Technical University	.....
Jury Members :	**Prof. Dr. Ahmet Dursun ALKAN** Yıldız Technical University	.....
	Doç. Dr. Erdem ÜÇER İstanbul Technical University	.....

Date of Submission : 02 May 2016
Date of Defense : 06 June 2016

To my family,

FOREWORD

I would like to express how grateful I am and thank my advisor, Prof. Şakir BAL. His guidance and encouragement throughout my graduate carrer has been instrumental.

I would like to thank my colleagues Ali DOĞRUL (PhD), Res. Assist. Ferdi ÇAKICI and Res. Assist. Ahmet YURTSEVEN for taking time out of their studies to assist me in this process. I am very thankful to Assist. Prof. Bekir ŞENER for moral support.

I am also grateful to Ezgi BAKIRCIOĞLU (M.D.) for her patience and support throughout this period.

Finally, I would like to thank my family for the love and support I have gotten over the years.

May 2016

Süleyman DUMAN
Naval Arch. & Marine Eng.

TABLE OF CONTENTS

Page

ABBREVIATIONS

BEM	**:** Boundary Element Method
CFD	**:** Computational Fluid Dynamics
CMT	**:** Circular Motion Test
DDG	**:** Guided Missile Destroyer
DMI	**:** Danish Maritime Institute
DOF	**:** Degree of Freedom
DTMB	**:** David Taylor Model Basin
EFD	**:** Experimental Fluid Dynamics
FVM	**:** Finite Volume Method
IBEM	**:** Iterative Boundary Element Method
IIHR	**:** Iowa Institite of Hydraulic Research
IMO	**:** International Maritime Organization
INSEAN	**:** Istituto Nazionale per Studied Esperienze di Architettura Navale
ITTC	**:** International Towing Tank Conference
KCS	**:** Kriso Container Ship
KVLCC	**:** Kriso Very Large Crude Carrier
MARIN	**:** Maritime Research Institute Netherlands
MC	**:** Maneuvering Committee
MMG	**:** Mathematical Model Group
PMM	**:** Planar Motion Mechanism
RANSE	**:** Reynolds-averaged Navier-Stokes Equations
RAT	**:** Rotating Arm Test
SNAME	**:** Society of Naval Architects and Marine Engineers
SST	**:** Shear Stress Transport
URANS	**:** Unsteady Reynolds-averaged Navier-Stokes
US	**:** United States
VOF	**:** Volume of Fluid Method

SYMBOLS

B_M	: Moulded breadth
C_B	: Block coefficient
Fn	: Froude number
I_x, I_y, I_z	: Moment of inertia
L_{BP}	: Length between perpendicular
L_{WL}	: Length of waterline
r	: Yaw angular velocity
Rn	: Reynolds number
T	: Draft
t	: Time
u, v	: Surge and sway velocity components
$\dot{u}$, $\dot{v}$	: Surge and sway accelerations
x_G, y_G, z_G	: Coordinates of gravity center
Y_v, N_v	: Hydrodynamic derivatives
β	: Drift angle
ρ	: Density
Δ	: Displacement
λ	: Scale factor
δ	: Rudder deflaction angle
ψ	: Heading angle
ϕ	: Heeling angle

LIST OF TABLES

Page

LIST OF FIGURES

Page

INVESTIGATION OF THE TURNING PERFORMANCE OF A SURFACE COMBATANT WITH URANS

SUMMARY

The prediction of ship-maneuvering performance have been challenging topics in ship hydrodynamics research due to its non-linear and highly complex nature. The turning maneuvering performance of a surface combatant is investigated with URANS method in this study. Numerical simulations of static PMM (Planar Motion Mechanism) tests are performed toward this goal by using a commercial RANSE solver software Star CCM+ in an unsteady manner. The fluid flow is considered as 3-dimensional, incompressible and fully turbulent. The free surface effect has been taken into account by including volume of fluid (VOF) method. Grid independence study is performed for 4 different grid quality. The effect of turbulence model is investigated by using two-equation models. The URANS and Eulerian approaches are investigated for several cases. The computational results, e.g., forces, moments, are used to determine the hydrodynamic derivatives according to Abkowitz's mathematical model. The acceleration and angular velocity derivatives are used as described in literature. The rudder terms are calculated from the results of "drift and rudder" simulations.

The prefered ship model is DTMB 5512, which is a 1/46.6 scale of US Navy DDG51 frigate, with L=3.048 m and geosim of DTMB 5415. Numerical analyses are performed in a 19.507m x 14.630m x 6.401m virtual towing tank for fixed condition. Hull is identified as a non-slip wall in order to dictate kinematic boundary condition. Front, top and bottom faces of the computational domain are defined as velocity inlets. Side faces are assigned as symmetry-planes and the back face is defined as pressure outlet. VOF wave is defined at draft of the ship as calm water.

Computational results are compared with the available experimental data. Turbulent kinetic energy and vorticity magnitude are observed on the plane sections normal to the x-direction for several cases. The results for two-equation turbulence models are examined and the suitable turbulence model for the presented study is selected. Wave profiles along the hull are plotted and compared with the EFD validation data. The viscous and inviscid flow results are compared with each other for several cases. Hydrodynamic derivatives are compared with the EFD results and empirical formulas and then are used as inputs to DYNEQNOMS (Dynamic Equations of Motion Solver), which is a custom developed computer program within the scope of this study to simulate ship turning maneuver. The turning maneuver performance parameters are compared with the literature.

BİR SU ÜSTÜ SAVAŞ GEMİSİNİN DÖNME PERFORMANSININ URANS KULLANILARAK İNCELENMESİ

ÖZET

Gemilerin manevra performanslarının belirlenmesi, karmaşık ve lineer olmayan doğası sebebiyle, gemi hidrodinamiği araştırmalarının zorlu konularından olmuştur. Bu sebeple yüzen bir cismin hidrodinamik performansının gerek nümerik gerekse deneysel olarak tahmin edilmesi büyük önem arz etmektedir. Genel olarak gemilerin manevra performansları; rota tutma veya değiştirme, manevra yapma ve hız değiştirme kabiliyetlerinin birleşiminden meydana gelmektedir. Rota değiştirme kabiliyeti özellikle savaş gemileri için önemli bir manevra karakteristiğidir. Dizayn aşamasında gemilerin manevra performanslarının tahmin edilebilmesi için pratik ve hızlı cevap verebilen bir çözüme duyulan ihtiyaç, CFD metodunun gemi manevra problemlerinde kullanılmasını teşvik etmiştir.

Bu çalışmada bir su üstü savaş gemisinin dönme manevrası performansı URANS metodu ile incelenmiştir. Bu amaç doğrultusunda, düzlemsel hareket mekanizması (PMM) yöntemi ile yapılan statik ve dinamik model deneylerinden, statik deneyler zamana bağlı olarak, ticari bir RANSE çözücü yazılım olan Star CCM+ ile gerçekleştirilmiştir.

Tez, beş ana bölümden oluşmaktadır. İlk bölümde tezin amacı, kapsamı, manevra performans hesaplarında kullanılan metodların tarihsel gelişimi, ITTC MC'nin manevra metodlarını sınıflandırma şekli ve IMO manevra standartları verilmiştir. İkinci bölümde gemilerin manevra denklemleri ve gemiye etkiyen kuvvet ve momentlerin hesaplanması için kullanılan matematiksel model, doğrusal rota stabilitesinin hesaplanması ve hidrodinamik türevlerin fiziksel yorumu ve nasıl hesaplanacağı açıklanmıştır. Üçüncü bölümde, hidrodinamik analizler için kullanılan URANS metodu, türbülans modelleri, ayrıklaştırma metodu ve çözüm metodolojisi verilmiştir. Dördüncü bölümde CFD analiz sonuçları ve dönme manevrası simülasyonundan elde edilen dönme performans parametreleri literatürdeki sonuçlar ile karşılaştırmalı olarak verilmiştir. Beşinci bölümde ise bu tez kapsamında kullanılan çözüm metodları ve elde edilen sonuçlar değerlendirilmiş olup, gelecekte yapılacak çalışmalara hakkında bilgi verilmiştir.

CFD analizlerinde akışın üç boyutlu, sıkıştırılamaz ve türbülanslı olduğu kabul edilmiş olup, serbest su yüzeyi etkisi VOF metodu ile hesaplara dahil edilmiştir. Ayrıklaştırma metodu olarak sonlu hacimler kullanılmıştır. Ağdan bağımsızlık çalışması, dört farklı ağ örgüsü kalitesi için yapılmıştır. Türbülans modelinin çözüme etkisi iki denklemli türbülans modelleri için araştırılmıştır. URANS ve Euler yaklaşımları bazı özel durumlar için incelenmiştir. Kuvvet ve momentler gibi sayısal sonuçlar, Abkowitz'in önerdiği matematik modele göre, hidrodinamik türevlerin hesaplanmasında kullanılmıştır. İvme ve açısal hıza bağlı hidrodinamik türevler literatürdeki sonuçlardan alınmıştır. Dümen terimleri "drift and rudder" simülasyon sonuçları kullanılarak hesaplanmıştır.

Gemi modeli olarak, Amerikan Donanması'na ait DDG51 firkateyninin 1/46.6 ölçekli ve L=3.048 boyundaki ve DTMB 5415 ile geometrik olarak benzer DTMB 5512 modeli kullanılmıştır. Nümerik analizler 19.507m x 14.630m x 6.401m boyutundaki sanal bir tankta, model hareketlerinin kısıtlandığı durum için gerçekleştirilmiştir. Gemi modeli, kinematik cisim şartını sağlatmak için kaymaz duvar sınır koşulu ile tanımlanmıştır. Hesaplama hacminin ön, üst ve dip yüzeylerine, akışkanın hesaplama hacmine giriş yaptığı yüzeyler olacak şekilde sınır koşulu tanımlanmıştır. Yan yüzeyler için simetri düzlemi sınır şartı atanmıştır ve arka yüzey akışkanın hesaplama hacmini terk ettiği çıkış yüzeyi olarak belirlenmiştir. Serbest su yüzeyi dalgaları gemi modelinin su çekimi yüksekliğinde sakin su şeklinde tanımlanmıştır. Serbest su yüzeyi dalgaların belli bir enine mesafe sonrasında sönümlendiği varsayılmıştır.

Hesaplama hacmini oluşturan ağ örgüsü genel olarak hexahedral (altı yüzlü) yapıdadır. Model etrafında akışın daha düzensiz hale gelmesinden dolayı ağ yapısında iyileştirmeler yapılmıştır. Özellikle modelin baş kısmında bulunan sonardom çevresinde, yalpa omurgaları civarında ve kıç kısmında daha sık ağ örgüsü oluşturulmuştur. Benzer şekilde serbest su yüzeyi deformasyonlarını doğru hesaplayabilmek için sakin su hattı bölgesinde daha sık ağ örgüleri ile çalışılmıştır. Model yüzeyinden belli bir mesafeye kadar sınır tabaka tanımlanmış ve bu bölgede ağ yapısı sıklaştırılmıştır. Ağdan bağımsızlık çalışması neticesinde sonsuz küçüklükte ağ elemanları atılsa da nümerik çözümün belli bir değere yakınsadığı görülmüştür. Mevcut bilgisayar gücü de dikkate alınarak hesaplamalar için uygun ağ örgüsü tercih edilmiş ve bütün analizlerde bu ağ örgüsü kullanılmıştır.

Hesaplamalı akışkanlar dinamiği metoduyla elde edilen sonuçlar literatürdeki deneysel veriler ile karşılaştırılmıştır. Gemi etrafındaki akış; serbest su yüzeyi deformasyonları, hidrodinamik kuvvetler ve momentler açısından incelenmiştir. Bunlara ek olarak türbülans kinetik enerjisi ve girdaplılık miktarı da normali x-yönünde olan ve gemi boyunca alınan düzlem kesitler üzerinde bazı özel durumlar için gözlenmiş ve ekte sunulmuştur. İki denklemli türbülans modelleri kullanılarak yapılan HAD analiz sonuçları tekneye etkiyen kuvvetler ve momentler baz alınarak karşılaştırılmıştır. Bu çalışma neticesinde, statik PMM simülasyonları için uygun olan türbülans modeli belirlenmiştir. Gemi boyunca oluşan dalga profilleri, boyuna kesitler alınarak çizdirilmiş ve literatürdeki deney sonuçları ile karşılaştırılmıştır. Viskoz ve viskoz olmayan akım kabulü ile gerçekleştirilen analizlerin sonuçları, serbest su yüzeyi deformasyonları ve hidrodinamik kuvvetler açısından birbirleriyle karşılaştırılmıştır. Beklendiği üzere viskoz olmayan durumdaki serbest su yüzeyi dalga genliklerinin, geminin kıç kısmında ve dümen suyu bölgesinde viskoz model sonuçlarına oranla daha yüksek olduğu görülmüştür. Özellikle yüksek hücum açılarında, viskoz olmayan çözümün sadece kıç bölgesinde değil gemi boyunca da sağlıklı olmayan sonuçlar verdiği gözlenmiştir.

Hidrodinamik analizler sonucunda tekneye etki eden kuvvet ve momentler hesaplanmıştır. Bunlar, matematik modelin önerdiği şekilde hidrodinamik türevlerin hesaplanmasında kullanılmıştır. Hidrodinamik türevler, deneysel veriler ve ampirik formüller ile karşılaştırılmış ve daha sonra bu çalışma kapsamında dönme manevrasını simüle etmek için geliştirilen DYNEQNOMS (Dynamic Equations of Motion Solver) bilgisayar programına girdi olarak kullanılmıştır. Geliştirilen bilgisayar programına girdi olarak hesaplamalı akışkanlar dinamiği analizlerinden elde edilen hidrodinamik türevlerin yanı sıra dümen açısı değerleri ve gemiye ait bazı temel değerler de kullanılmıştır. Gemi manevralarının simüle edilebilmesi için iki ötelenme (surge, sway) ve bir dönme (yaw) hareketinden oluşan gemi manevra denklemleri, Euler

metodu ile çözülmek üzere matris formuna getirilmiştir. Hareket denklemlerinde gemiye etkiyen kuvvet ve momentler Abkowitz'in önerdiği üçüncü mertebeden Taylor Serisi açılımı ile hesaplanmıştır. Elde edilen matris Gauss-Jordan Eliminasyon metodu yardımı ile her bir zaman adımında çözülmüş ve modele ait çizgisel ve açısal hız değerleri hesaplanmıştır. Hesaplanan her bir hız değeri bir sonraki zaman adımında kullanılmak üzere hareket denklemlerinde yerine yazılmıştır. Başlangıç koşulu olarak geminin belli bir hızda ileri doğru ötelenme (surge) hareketini yaptığı ve diğer hareketlere ait hız ve ivme değerlerinin sıfır olduğu kabul edilmiştir.

Modele ait çizgisel ve açısal hız değerleri her bir zaman adımında bilindiğinden rotadan sapma açısı, kayma açısı, dönme dairesi çapı, modelin başlangıçtaki hareket doğrultusunda katettiği mesafe ve modelin başlangıçtaki hareket doğrultusuna dik (enine) yönde katettiği mesafe hesaplanmıştır. Hesaplanan bu değerlerden sabit dönme dairesi çapı, lineer model ve ampirik formüller ile kıyaslanmıştır. Modele ait taktik çapı da literatürdeki sonuçlar ile karşılaştırılmıştır.

1. INTRODUCTION

Prediction of ship-maneuvering performance have been one of the most challenging topics in ship hydrodynamics research because of its highly complex unsteady and non-linear nature. The general ship hydrodynamics can be devided into two main part (Sabuncu, 1985):

- Controlling the ship's motion in a desired manner (ship-maneuvering).
- Noncontrollable ship motions arising from external forces (seakeeping).

Knowing the maneuvering characteristics of a ship allows us to control the ship's motion in a desired manner. The controllability can be necessary for either navy, e.g., setting the trajectory of a surface combatant in a specific course when following an enemies boat, or a cargo ship to maneuver safely in a harbour etc. Whatever the vessel type, controllability means regulating a ship's trajectory, changing course, reduce or increase speed, in general terms, controlling the orientation of a ship at sea. To gather up, the controllability comprises starting, steering a steady course, turning, slowing, stopping, backing and diving (for submarines). Figure 1.1 represents a control loop for conventional ships.

The study of the complex subject of controllability is usually divided into three distinct areas (Lewis, 1989):

- Coursekeeping (or steering): The important factor is to maintain a steady mean course or heading.
- Maneuvering: The controlled change in the direction of motion, i.e., turning or course changing. The important factors are the radius of turning motion and the distance required to accomplish the change.
- Speed changing: Stopping and backing or speed reduction because of external factors are the scenarios for speed changing. The important factors are rapidity and the distance covered in accomplishing changes.

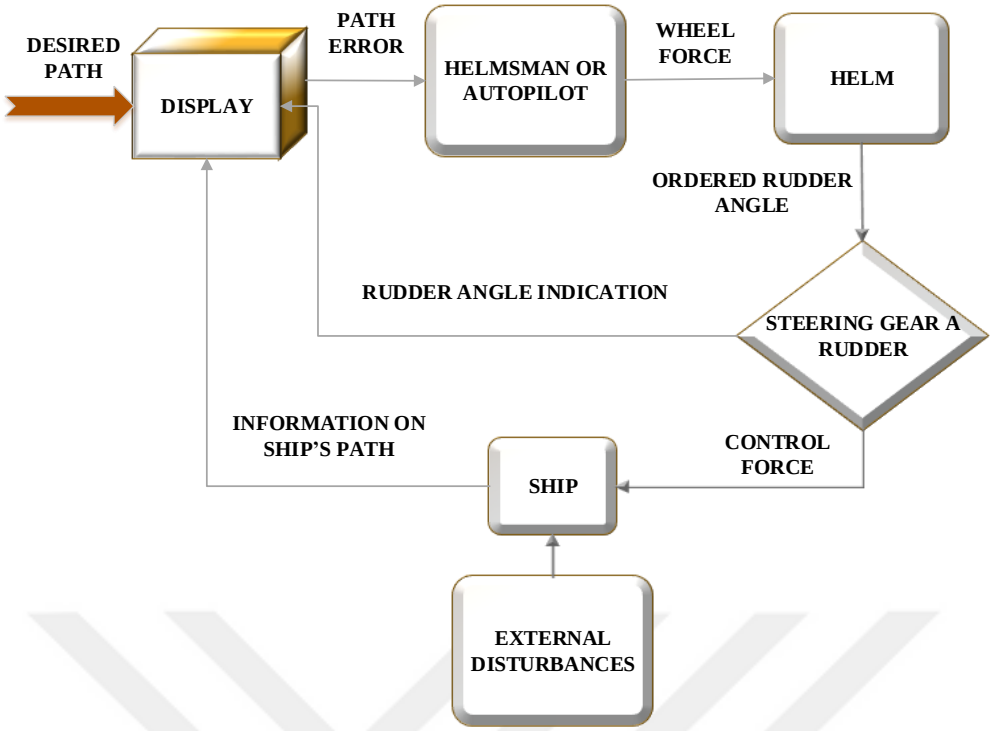

Figure 1.1 : Closed-loop control system of a ship.

For conventional ships, coursekeeping and maneuvering may tend to work against each other; an easy turning ship may be difficult to keep on course whereas a ship which maintains course well may be hard to turn. The optimization is needed here in order to ensure that the demanding requirements are satisfied.

Maneuvering requirements are a standart part of the contract between shipyard and shipowner. Although the minimum requirements for all ships are specified by IMO regulations, shipowners may introduce additional or more severe requirements for certain ship types, e.g., tugs, ferries, exploration ships (Bertram, 2012).

1.1 Motivation

It is crucial to estimate the hydrodynamic performance of a floating vessel numerically or experimentally. As known, the experimental methods are expensive and time consuming. Also there are several uncertainties caused by the experimental measurement equipments. Meanwhile, numerical methods are cost effective as compared with the experiments and are quick-responding methods. In addition to this, computational fluid dynamics (CFD) methods can be employed for both simulating inviscid and viscous flows.

The course changing ability of the ship is an important maneuvering characteristic especially for the surface combatants and is expressed by the turning circle maneuver (Faltinsen, 2006). The need to a practical and quick-responding solution for the assessment of ship-maneuvering performance at design stage encouraged the author to use CFD methods to investigate the turning maneuvering performance of a surface combatant. It is hoped that the presented study will contribute to the future studies in the field of ship-maneuvering.

1.2 Purpose of Thesis

The objective of this research is to investigate turning maneuvering characteristics of a surface combatant US Navy DDG51 by performing URANS simulations. The model used for this purpose is DTMB 5512, a length of L=3.048 m and a geosim of DTMB 5415 for the US Navy DDG51. The model is un-appended except for port and starboard bilge keels, i.e., not equipped with shaft, struts, propellers, or rudders as is used in PMM model tests at IIHR (Yoon et al., 2015).

The hydrodynamic forces and moments acting on the hull are calculated with URANS method and then are used to determine hydrodynamic forces. Finally, the hydrodynamic derivatives including rudder terms are used to solve the simultaneous differential equations of motion to simulate the turning maneuvering of DTMB 5512.

1.3 Scope of the Thesis

To assess the turning maneuvering performance of DTMB 5512, static PMM tests have been conducted by using a commercial RANS solver in an unsteady manner. Finite volume method (FVM) is used as a discretization technique. The fluid flow is considered 3D, incompressible and fully turbulent. Free surface effect has been taken into acount by using volume of fluid method (VOF). Since ship-maneuvering is traditionally handled in calm water condition (Faltinsen, 2006), the free surface is considered as calm water in the simulations. The grid independence study is performed for 4 different grid quality. Two-equation turbulence models are compared with eachother and appropriate model is chosen to be used in the rest of the simulations. To investigate the effect of viscosity, several cases have been simulated both with

URANS and Euler methods and the results are compared with eachother and with the available experimental data.

General PMM testing technique, which is recommended by FORCE, enables various test conditions to be studied individually. These conditions are “static rudder”, “static drift”, “static drift and rudder”, “static heel”, “static heel and drift”, “pure sway”, “pure yaw”, “yaw and rudder”, “yaw and drift” and “yaw and heel” (DMI, 2000; Simonsen et al., 2012). “Pure yaw”, “pure sway” and combinations with one of these tests are harmonic tests where the ship model is forces to move in a certain trajectory. In the remaining tests the ship model is fixed at a certain position, e.g., at an angle of attack (static drift) or at a roll angle (static heel).

In this study, “static drift”, “static rudder” and “drift and rudder” ship model tests are simulated with URANS method. Althought the heave, pitch and roll motions play significant role for the assessment of seakeeping performance (Bhattacharyya, 1978), e.g., investigation of transverse stability (Ucer, 2011), surge, sway and yaw motions are considered in the first place for ship-maneuvering motions. Therefore, the turning maneuvering motion is considered three degree of freedom. The heave, pitch and roll motion equations have not been employed. The simulation cases are given in Chapter 4 in detail. The hydrodynamic forces and moments acting on the hull are calculated with URANS method for each case, then are used to determine maneuvering coefficients. The harmonic derivatives are used as described in Yoon (2009). The hydrodynamic derivatives are put into the Abkowitz’s mathematical model (Abkowitz, 1964).

Finally, a computer program called as DYNEQNOMS is developed in MATLAB to solve the simultaneous differential equations of motion to simulate the turning maneuver of DTMB 5512. Turning maneuver performance parameters such as steady turning diameter and tactical diameter are compared both with the available validation data and empirical formulas.

1.4 Literature Review

Traditional perspective to predict ship-maneuvering has been either empirical methods using databases or experimental model tests. Generally, empirical database methods use mathematical model and hydrodynamic derivatives based on either empiricism or

mixed semi-theoretical and semi-empirical methods. In recent years, computational fluid dynamics (CFD) based methods began to gain importance for investigating ship maneuvering performance, for both viscous and inviscid fluid flows.

1.4.1 Overview of maneuvering prediction methods

The methods include the cross flow drag model (Hooft, 1994), database regression methods such as, Norrbin (1971), Inoue, Hirano, and Kijima (1981) and Clarke et. al. (1983), the Kijima method (Kijima et. al., 2003), and more recently the combined slender body and the cross flow drag theories (Martinussen et. al., 2008 and Toxopeus et. al., 2008). Most of the time, empirical database methods are relatively simple and giving quick results. However, if principle dimensions of the ship handled are outside the database, this method will not response in a healthy way.

Experimental ship model tests can be separated into free running model tests and captive model tests (Lewis, 1989). In the free-running model test, a scaled model that is self-propelled and self-steered model performs prespecified maneuvers such as spiral, zig-zag, or turning maneuvers. In all types of model tests, free-running model test is the closest to the reality, due to the fact that there is no mathematical modeling or assumption to simplify the problem. Nevertheless, as yield only the final results/information, free-running tests give less detail about the individual maneuvering factors (such as, changes according to the steering angle of sway forces). Recent studies to extract more information from free-running model testing results, so-called the system identification method, show progress by using either mathematical models (Oltmann, 2000; Viviani et al., 2003; Artyszuk, 2003; and Yoon et. al., 2003) or a Neural Network logic (Moreira and Guedes Soares, 2003). The other ship model test so-called captive model testing comprises planar motion mechanism (PMM) test (Gertler, 1966, and Strom-Tejsen and Chislett, 1966), rotating arm test (or circular motion mechanism, CMT) and oblique towing test. Captive model testing is conducted according to various mathematical models developed for the ship motion equations, of which hydrodynamic derivatives are determined experimentally.

In addition to traditional methods, in recent years, computational fluid dynamics (CFD) based methods began to gain importance for computing hydrodynamic forces, which are used to calculate maneuvering coefficients, for both viscous and inviscid fluid flows. The steady flow characteristics around 3-dimensional cavitating or

noncavitating bodies are investigated by a nonlinear iterative boundary element method (IBEM) which is based on Greens's theorem (Bal, 2008a). Bal (2008b), used an iterative boundary element method (IBEM) to predict the wave pattern and wave resistance of surface piercing bodies. An iterative boundary element method (IBEM) was developed to predict the flow characteristics such as; wave drag and lift, for both 2-D and 3-D cavitating hydrofoils and ship-like bodies moving with constant speed under or on the free surface (Uslu and Bal, 2008). The wave deformations caused by a point source moving under free surface have been investigated by boundary element method (BEM) (Dogrul, 2015). Besides potential based studies, significant progress has been made toward viscous flow calculations by applying Reynolds-averaged Navier-Stokes (RANS) based CFD codes to static maneuvers (Tahara et. al., 2002; Simonsen and Stern 2003; Toxopeus, 2006; Simonsen et. al., 2006; Bhushan et al., 2007), to dynamic maneuvers (Kim and Rhee, 2002; Di Mascio and Broglia, 2003; Broglia et. al., 2006; Sakamoto, 2009; Kim et. al., 2015), and to trajectories or more direct six-degree-of-freedom (6-DOF) maneuvering predictions (Carrica and Stern, 2008), with generally good agreement with experimental data. The wave deformations along the hull have been investigated for particularly high Froude numbers by using RANS based CFD method (Dogrul and Celik, 2016).

The CFD simulations provide detailed information about the entire flow structure around the hull. Forces and moments are computed during the simulations and then they are used to determine maneuvering coefficients. There are some difficulties right along with the advantages of URANS method such as; the implementation of complex geometries, solving 6-DOF ship motions (needs huge computing capability) and environmental effects etc. Moreover, RANS methods are required to be verified and validated (V&V, Stern et al., 2001) to be reliable and accepted by end-users as a solution tool for use in industry or the navy. Simulating the real world needs validation data carried out from experiments. The lack of available experimental fluid dynamics (EFD) validation data, especially for ship motions and maneuvering, makes it harder for V&V of RANS solvers.

Recently, international workshops are organized via collaboration of related institutions to meet the demand for EFD validation data. Researches about ship maneuvering have focused on modern tanker (KVLCC1 and KVLCC2), Kriso Container Ship (KCS), and US Navy surface combatant (DTMB 5415), which is

currently used in this study, hull forms as per the Gothenburg 2000 Workshop Larsson et. al. (2003) and Kim et. al. (2001) provided steady-flow data for KVLCC2 and KCS. For DTMB 5415, data procurement has been part of an international collaboration between IIHR, INSEAN and DTMB, for more than 10 years (Yoon, 2009). After the Gothenburg Workshop, SIMMAN 2008 Workshop was organized to discuss more recent efforts. The purpose of the workshop was to benchmark the prediction capabilities of different ship maneuvering simulation methods including the system-based and CFD-based methods through comparisons with results.

1.4.2 24th ITTC MC

The 24th ITTC Maneuvering Committee (MC) reviewed state-of-the-art progress in maneuvering predictios and categorized typical maneuvering prediction methods into three groups (Figure 1.2):

- No Simulation
- System Based Simulation
- CFD Based Simulation methods.

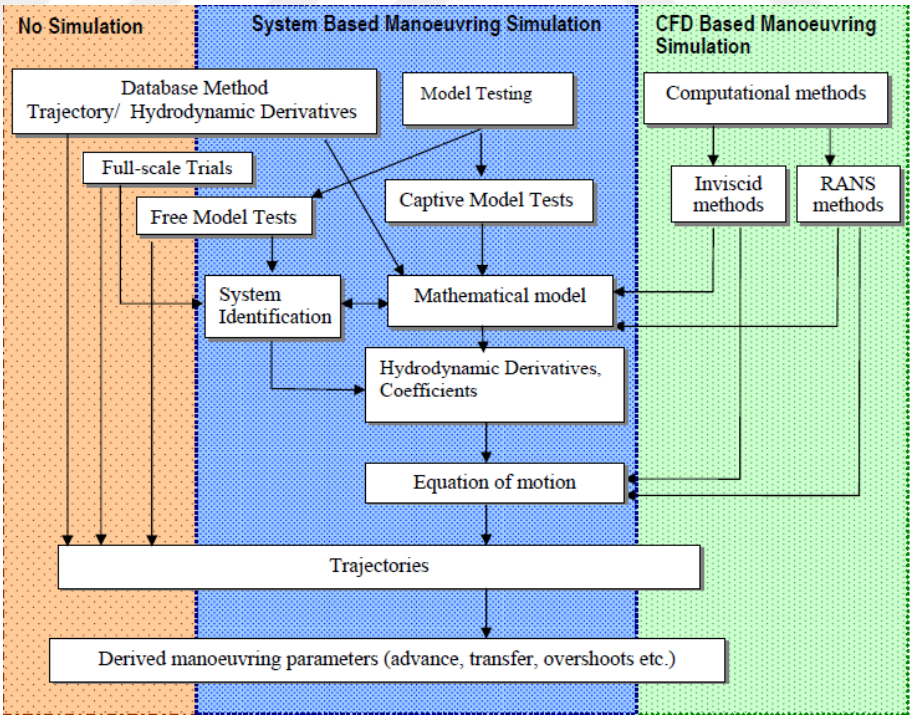

Figure 1.2 : Categorization of typical maneuvering prediction methods.

The No Simulation method needs no mathematical model. All maneuvering parameters such as ship advance, transfer, tactical diameter and etc. are calculated by

using a database from full-scale ship trials or model-scale free-running model test by measuring the ship trajectories.

Contrarily, the System Based Simulation method, simulates the ship trajectories by solving the equations of motion. For this purpose, various mathematical models have been developed up till today. One of the well-known mathematical model, which is basis of this study, is Abkowitz's Taylor series of expansion.

The System Based Simulation method includes:

- Database
- Model testing
- System identification method.

The databases of full and/or model scale test results are generally used to establish an empirical formula or regression equations to obtain hydrodynamic derivatives (Norrbin, 1971; Inoue et. al., 1981; Clarke et. al., 1983; Kijima et al., 1990 and 1993). Besides, these empirical formulas and/or regression equations can be used together with theoretical models such as the Japanese Mathematical Model Group (MMG) model (Kijima et al., 1993) or the cross-flow drag model (Hooft, 1994).

Another method is model testing, which is divided into free-running and captive model tests. The procedure for these model tests are well defined in the captive model test procedure (ITTC, 2002) and free-running model test procedure (ITTC, 2014).

The CFD Based Simulation method gives opportunity to simulate the ship's trajectory as free-running model tests do and the captive model tests, which are based on mathematical modeling of motion equations. This method is similar to the System Based Simulation method in terms of calculating the hydrodynamic derivatives of the mathematical models or to solve the motion equations directly.

1.4.3 IMO maneuvering standarts

The standart maneuvers should be performed without the use of any maneuvering aids which are not continuously and readily available in normal operation (IMO, 1993).

In order to evaluate the performance of a ship, maneuvering trials should be conducted to both port and starboard and at condifitons specified below:

- Deep, unrestricted water;

- Calm environment;
- Full load (summer load line draught), even keel condition;
- Steady approach at the test speed.

The maneuverability of the ship is considered satisfactory if the following criteria are complied with:

a. Turning ability

The advance should not exceed 4.5 ship lengths (L) and the tactical diameter should not exceed 5 ship lengths in the turning circle manoeuvre.

b. Initial turning ability

With application of 10° rudder angle to port/starboard, the ship should not have travelled more than 2.5 ship lengths by the time the heading has changed by 10° from original heading.

c. Yaw checking ability

The value of the first overshoot angle in the 10°/10° zig-zag test should not exceed:

i. 10° if L/V is less than 10 s;

ii. 20° if L/V is 30 s or more;

iii. (5+1/2(L/V)) degrees if L/V 10 s or more, but less than 30 s, where L and V are expressed in m and m/s, respectively.

The value of the second overshoot angle in the 10°/10° zig-zag test should not exceed:

i. 25° if L/V is less than 10 s;

ii. 40° if L/V is 30 s or more;

iii. (17.5+0.75(L/V)) degrees if L/V 10 s or more, but less than 30 s.

The value of the first overshoot angle in the 20°/20° zig-zag test should not exceed 25°.

d. Stopping ability

The track reach in the full astearn stopping test should not exceed 15 ship lengths. However, this value may be modified by the administration where ships of large displacement make this criterion impracticable, but should in no case exceed 20 ship lengths.

2. MATHEMATICAL MODEL

2.1 General Equations of Motion

The generalized 6-DOF rigid-body equations of motion in a body-fixed, non-inertial frame of reference xyz that is moving relative to an Earth-fixed, inertial reference frame $x_0 y_0 z_0$ (Figure 2.1) can be derived as (Fossen, 1994):

$$m\left[\dot{u} - vr + \omega q - x_G\left(q^2 + r^2\right) + y_G\left(pq - \dot{r}\right) + z_G\left(pr + \dot{q}\right)\right] = X \tag{2.1a}$$

$$m\left[\dot{v} - \omega p + ur - y_G\left(r^2 + p^2\right) + z_G\left(qr - \dot{p}\right) + x_G\left(qp + \dot{r}\right)\right] = Y \tag{2.1b}$$

$$m\left[\dot{\omega} - uq + vp - z_G\left(p^2 + q^2\right) + x_G\left(rp - \dot{q}\right) + y_G\left(rq + \dot{p}\right)\right] = Z \tag{2.1c}$$

$$\begin{aligned} I_x\dot{p} + \left(I_z - I_y\right)qr - \left(\dot{r} + pq\right)I_{xz} + \left(r^2 - q^2\right)I_{yz} + \left(pr - \dot{q}\right)I_{xy} \\ + m\left[y_G\left(\dot{\omega} - uq + vp\right) - z_G\left(\dot{v} - \omega p + ur\right)\right] = K \end{aligned} \tag{2.1d}$$

$$\begin{aligned} I_y\dot{q} + \left(I_x - I_z\right)rp - \left(\dot{p} + qr\right)I_{xy} + \left(p^2 - r^2\right)I_{zx} + \left(qp - \dot{r}\right)I_{yz} \\ + m\left[z_G\left(\dot{u} - vr + \omega q\right) - x_G\left(\dot{\omega} - uq + vp\right)\right] = M \end{aligned} \tag{2.1e}$$

$$\begin{aligned} I_z\dot{r} + \left(I_y - I_x\right)pq - \left(\dot{q} + rp\right)I_{yz} + \left(q^2 - p^2\right)I_{xy} + \left(rq - \dot{p}\right)I_{zx} \\ + m\left[x_G\left(\dot{v} - \omega p + ur\right) - y_G\left(\dot{u} - vr + \omega q\right)\right] = N \end{aligned} \tag{2.1f}$$

The first three equations represent the translational motion; surge-x, sway-y and heave-z while the last three equations represent the rotational motion; roll-ϕ, pitch-θ and yaw-ψ, respectively.

The origin of ship-fixed reference frame is located at the gravity center of the ship (Figure 2.1). Right hand side of the 6-DOF equations of motion represents the forces and moments; X, Y, Z are the external forces acting on the vessel and K, M, N are the external angular moments respectively. m is the mass of the vessel and I_x, I_y, I_z are the moments of inertia of the vessel wrt each axis. The center of gravity of the vessel is given at the point defined with x_G, y_G, z_G on the earth-fixed reference frame.

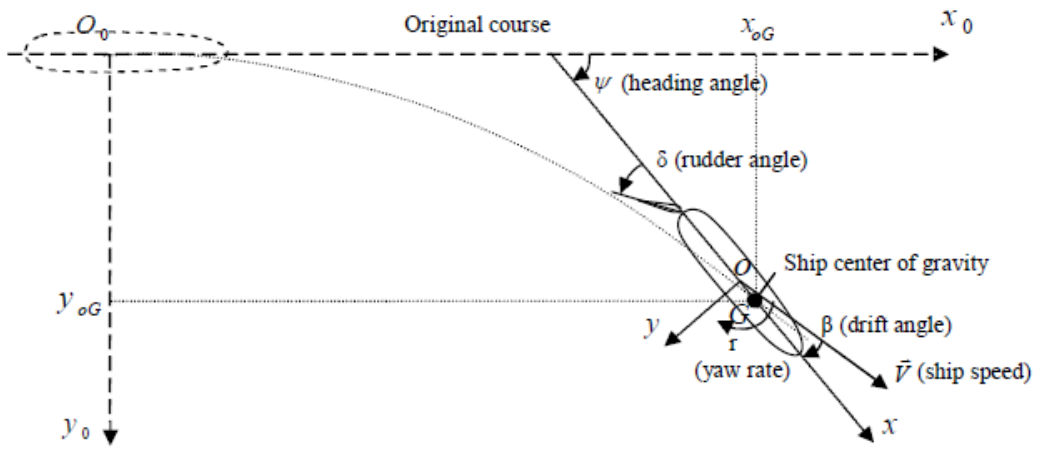

Figure 2.1 : Coordinate systems.

The translational velocities and accelerations are given below for each axes:

$$\left\{\begin{array}{ll}\dot{x}=u & \rightarrow \text{surge velocity}\\ \dot{y}=v & \rightarrow \text{sway velocity}\\ \dot{z}=\omega & \rightarrow \text{heave velocity}\end{array}\right\}\xrightarrow{\frac{d}{dt}}\left\{\begin{array}{ll}\ddot{x}=\dot{u} & \rightarrow \text{surge acceleration}\\ \ddot{y}=\dot{v} & \rightarrow \text{sway acceleration}\\ \ddot{z}=\dot{\omega} & \rightarrow \text{heave acceleration}\end{array}\right\}$$

The rotational velocities and accelerations are given below for each axes:

$$\left\{\begin{array}{ll}\dot{\phi}=p & \rightarrow \text{roll rate}\\ \dot{\theta}=q & \rightarrow \text{pitch rate}\\ \dot{\psi}=r & \rightarrow \text{yaw rate}\end{array}\right\}\xrightarrow{\frac{d}{dt}}\left\{\begin{array}{ll}\ddot{\phi}=\dot{p} & \rightarrow \text{roll acceleration}\\ \ddot{\theta}=\dot{q} & \rightarrow \text{pitch acceleration}\\ \ddot{\psi}=\dot{r} & \rightarrow \text{yaw acceleration}\end{array}\right\}$$

For surface ships moving on unbounded and calm water, forces and moments acting on the hull are in the horizontal plane. Hence, the heave, roll and pitch motions can be neglected such that $\omega = p = q = \dot{\omega} = \dot{p} = \dot{q} = 0$. Due to symmetry of the vessel in the xz-plane, $y_G = 0$. The equations of motion for surface ships take the following form when these simplifications are made:

$$m\left(\dot{u} - vr - x_G r^2\right) = X \tag{2.2a}$$

$$m\left(\dot{v} + ur + x_G \dot{r}\right) = Y \tag{2.2b}$$

$$I_z \dot{r} + m x_G \left(\dot{v} + ur\right) = N \tag{2.2c}$$

for surge, sway and yaw, respectively.

2.2 Equations of Ship Maneuvering Motion in a Moving Reference Frame

The basic equations of motion (2.1) are described using Newton's second law of motion. Basic equations in the horizontal plane can be established with two sets of axes either. First set of axes is earth-fixed and the second one is ship-fixed.

Referring to the first axes fixed in the earth, the Newtonian equations of motion of the ship are:

$$X_0 = \Delta \ddot{x}_{OG} \tag{2.3a}$$

$$Y_0 = \Delta \ddot{y}_{OG} \tag{2.3b}$$

$$N = I_Z \ddot{\psi} \tag{2.3c}$$

where the two dots above the symbols x_{OG}, y_{OG} and ψ indicate the second derivatives of those values with respect to time, t. X_0 and Y_0 are total forces in x_0 and y_0 directions, respectively. Δ is mass of the ship (displacement tonnage). N represents the total moment about an axis through the center of gravity of ship and parallel to the z_0-axis. I_Z is mass moment of inertia of ship about the z_0-axis, and finally ψ indicates yaw angle in the horizontal plane measured from the vertical $x_0 z_0$ plane to the x-axis of the ship.

Althought the equations (2.3) are simple to use, expressing these equations in ship-fixed moving reference frame is more convinient for a ship moving relative to earth-fixed coordinate system.

In order to convert equations (2.3) from axes fixed in the earth to axes fixed in the moving ship, the total forces X and Y in the x and y-directions, respectively, are expressed in terms of X_0 and Y_0 (Lewis, 1989):

$$X = X_0 \cos\psi - Y_0 \sin\psi \tag{2.4a}$$

$$Y = X_0 \sin\psi + Y_0 \cos\psi \tag{2.4b}$$

likewise

$$\dot{x}_{OG} = u\cos\psi - v\sin\psi \tag{2.5a}$$

$$\dot{y}_{OG} = u\sin\psi + v\cos\psi \tag{2.5b}$$

where the dot above the symbols indicates the first derivative of the related quantity with respect to time, and u and v are the components of ship's velocity V along x and y, respectively. If one more derivative of equations (2.5) is taken, accelerations can be written in the following forms:

$$\ddot{x}_{OG} = \dot{u}\cos\psi - \dot{v}\sin\psi - \left(u\sin\psi + v\cos\psi\right)\dot{\psi} \tag{2.6a}$$

$$\ddot{y}_{OG} = \dot{u}\sin\psi + \dot{v}\cos\psi + \left(u\cos\psi - v\sin\psi\right)\dot{\psi} \tag{2.6b}$$

Substituting equation (2.6) in equation (2.3) and inserting the resulting values of X_0 and Y_0 in equation (2.4) yields the following expressions:

$$X = \Delta\left(\dot{u} - v\dot{\psi}\right)$$

$$Y = \Delta\left(\dot{v} + u\dot{\psi}\right)$$

The last two equations obtained and the third equation of (2.3) express the equations of motin in the horizontal plane with the assumption of zero roll, pitch and heave. Thus, 3-DOF equations of motion in the horizontal plane can be written as:

$$X = \Delta\left(\dot{u} - v\dot{\psi}\right) \tag{2.7a}$$

$$Y = \Delta\left(\dot{v} + u\dot{\psi}\right) \tag{2.7b}$$

$$N = I_Z\ddot{\psi} \tag{2.7c}$$

As will be realised that equation (2.2) and (2.7) are the same except for the x location of gravity is non-zero in equation (2.2). These two sets of equations are obtained in a slightly different way. First set is come from the generalized equations of motion making simplifications and assumptions. The second set is procured with writing the Newton's second law of motion for 3-DOF and performing coordinate transformation.

There is a small difference arising from additional terms, between the equation (2.3) and (2.7). These terms are $\Delta v\dot{\psi}$ and $\Delta u\dot{\psi}$ called as centrifugal-force terms which result from the moving reference frame. In the earth-fixed axes, these terms are not considered.

In the presented study, equations (2.7) is employed where the origin of the moving reference frame is located at the center of gravity.

2.3 Forces and Moments Acting on a Vessel During Maneuver

The left hand side of the equation (2.7) are represents the forces and moments built up of four types of forces that act on a ship during a maneuver (Lewis, 1989):

- Hydrodynamic forces resulting from ship velocity and acceleration, rudder deflection and propeller rotation.
- Inertial reaction forces caused by ship acceleration (this type of force can be considered as the added mass in the seakeeping problems).
- Environmental forces due to wind, waves and currents.
- External forces such as tugs or thrusters.

The simple case of controllability is taken into account in this study. Hence, the last two type of forces are not included in the calculations due to assumptions of unbounded, deep and calm water (without wind, waves, current and external forces).

Hydrodynamic forces can be separated into two groups which arise from ship velocity (damping forces) and ship accelerations (added mass forces). The inertial reactions that are needed to balance the added mass forces called as d'Alembert forces and moments.

The deflection of a rudder effects the ship indirectly on turning motion. When the deflection begins, the rudder induces a moment that causes the ship to change its trajectory and to have an angle of attack (leeway angle) to the direction of motion of the center of gravity. Afterwards, hydrodynamic forces generated on the hull cause a change of lateral movement of the center of gravity. During this motion, ship is opposed by the inertial reactions. If the rudder remains at a fixed angle δ, a steady turning condition will evolve when hydrodynamic and inertial forces and moments come into balance (Lewis, 1989).

2.4 Mathematical Model and Hydrodynamic Derivatives

There are two kinds of manner for expression of the hydrodynamic force and moment, one is that introduced first by Prof. Martin A. Abkowitz from MIT in USA and the other one is due to the Mathematical Modeling Group (MMG) from Japan (Yoshimura, 2005).

In 1964, Prof. Abkowitz proposed a method for expression of the hydrodynamic forces and moments acting on a ship by using the Taylor Series expansion. The hydrodynamic forces and moments are expressed as functions of the kinematical parameters and the rudder angle in the following form:

$$X = F_X\left(u, v, r, \dot{u}, \dot{v}, \dot{r}, \delta\right) \tag{2.8a}$$

$$Y = F_Y\left(u, v, r, \dot{u}, \dot{v}, \dot{r}, \delta\right) \tag{2.8b}$$

$$N = N\ \left(u, v, r, \dot{u}, \dot{v}, \dot{r}, \delta\right) \tag{2.8c}$$

and then expanded in Taylor Series about the initial steady state of forward motion with constant speed, i.e., $u_0 = U$, $v_0 = 0$, $\dot{u}_0 = 0$, $\dot{v}_0 = 0$, $r_0 = 0$, $\dot{r}_0 = 0$, $\delta_0 = 0$. It results in:

$$\begin{aligned} X = X_0 &+ \frac{\partial X}{\partial u}(u-V) + \frac{\partial X}{\partial v}v + \frac{\partial X}{\partial r}r + \frac{\partial X}{\partial \dot{u}}\dot{u} + \frac{\partial X}{\partial \dot{v}}\dot{v} + \frac{\partial X}{\partial \dot{r}}\dot{r} + \frac{\partial X}{\partial \delta}\delta \\ &+ \frac{1}{2!}\left[\frac{\partial X}{\partial u}(u-V) + \frac{\partial X}{\partial v}v + \frac{\partial X}{\partial r}r + \frac{\partial X}{\partial \dot{u}}\dot{u} + \frac{\partial X}{\partial \dot{v}}\dot{v} + \frac{\partial X}{\partial \dot{r}}\dot{r} + \frac{\partial X}{\partial \delta}\delta\right]^2 X \\ &+ \ldots + \frac{1}{\mathrm{n}!}\left[\frac{\partial X}{\partial u}(u-V) + \frac{\partial X}{\partial v}v + \frac{\partial X}{\partial r}r + \frac{\partial X}{\partial \dot{u}}\dot{u} + \frac{\partial X}{\partial \dot{v}}\dot{v} + \frac{\partial X}{\partial \dot{r}}\dot{r} + \frac{\partial X}{\partial \delta}\delta\right]^n X + \ldots \end{aligned} \tag{2.9a}$$

$$\begin{aligned} Y = Y_0 &+ \frac{\partial Y}{\partial u}(u-V) + \frac{\partial Y}{\partial v}v + \frac{\partial Y}{\partial r}r + \frac{\partial Y}{\partial \dot{u}}\dot{u} + \frac{\partial Y}{\partial \dot{v}}\dot{v} + \frac{\partial Y}{\partial \dot{r}}\dot{r} + \frac{\partial Y}{\partial \delta}\delta \\ &+ \frac{1}{2!}\left[\frac{\partial Y}{\partial u}(u-V) + \frac{\partial Y}{\partial v}v + \frac{\partial Y}{\partial r}r + \frac{\partial Y}{\partial \dot{u}}\dot{u} + \frac{\partial Y}{\partial \dot{v}}\dot{v} + \frac{\partial Y}{\partial \dot{r}}\dot{r} + \frac{\partial Y}{\partial \delta}\delta\right]^2 Y \\ &+ \ldots + \frac{1}{\mathrm{n}!}\left[\frac{\partial Y}{\partial u}(u-V) + \frac{\partial Y}{\partial v}v + \frac{\partial Y}{\partial r}r + \frac{\partial Y}{\partial \dot{u}}\dot{u} + \frac{\partial Y}{\partial \dot{v}}\dot{v} + \frac{\partial Y}{\partial \dot{r}}\dot{r} + \frac{\partial Y}{\partial \delta}\delta\right]^n Y + \ldots \end{aligned} \tag{2.9b}$$

$$\begin{aligned} N = N_0 &+ \frac{\partial N}{\partial u}(u-V) + \frac{\partial N}{\partial v}v + \frac{\partial N}{\partial r}r + \frac{\partial N}{\partial \dot{u}}\dot{u} + \frac{\partial N}{\partial \dot{v}}\dot{v} + \frac{\partial N}{\partial \dot{r}}\dot{r} + \frac{\partial N}{\partial \delta}\delta \\ &+ \frac{1}{2!}\left[\frac{\partial N}{\partial u}(u-V) + \frac{\partial N}{\partial v}v + \frac{\partial N}{\partial r}r + \frac{\partial N}{\partial \dot{u}}\dot{u} + \frac{\partial N}{\partial \dot{v}}\dot{v} + \frac{\partial N}{\partial \dot{r}}\dot{r} + \frac{\partial N}{\partial \delta}\delta\right]^2 N \\ &+ \ldots + \frac{1}{\mathrm{n}!}\left[\frac{\partial N}{\partial u}(u-V) + \frac{\partial N}{\partial v}v + \frac{\partial N}{\partial r}r + \frac{\partial N}{\partial \dot{u}}\dot{u} + \frac{\partial N}{\partial \dot{v}}\dot{v} + \frac{\partial N}{\partial \dot{r}}\dot{r} + \frac{\partial N}{\partial \delta}\delta\right]^n N + \ldots \end{aligned} \tag{2.9c}$$

X_0, Y_0 and N_0 are the steady state values X, Y, N, respectively. For a ship moving forward at a constant speed, X_0 will be zero due to the balance between the total resistance of ship and thrust T. The derivatives in equation (2.9) are called as hydrodynamic derivatives. In the simplified derivative notation of SNAME (Nomenclature, 1952) these derivatives can be expressed as:

$$\frac{\partial X}{\partial u} = X_u, \quad \frac{\partial X}{\partial v} = X_v, \quad \frac{\partial X}{\partial r} = X_r, \quad \frac{\partial X}{\partial \dot{u}} = X_{\dot{u}}, \quad \frac{\partial X}{\partial \dot{v}} = X_{\dot{v}}, \quad \frac{\partial X}{\partial \dot{r}} = X_{\dot{r}}, \quad \frac{\partial X}{\partial \delta} = X_\delta,$$

$$\frac{\partial^2 X}{\partial u^2} = X_{uu}, \frac{\partial^2 X}{\partial v \partial u} = X_{uv} \; ; \ldots ,$$

and so on. Substituting equation (2.9) into equation (2.7), the equations of ship maneuvering motion yields the well-known Abkowitz model, or whole ship model which is employed in this study to simulate turning maneuver of DTMB model 5415.

Abkowitz (1964) also proposed to use a 3^{rd} -order Taylor Series expansion of the equation (2.9) with the following additional assumptions:

a. Forces and moments have symmetry in xz-plane except for a constant force and moment caused by the propeller, and

b. There are no second- or higher-order acceleration terms, and cross-coupling between acceleration and velocity parameters is negligible,

as per re-stated by Strom-Tejsen and Chislett (1966). Considering these assumptions, for small disturbances and at a constant forward speed, the Abkowitz's mathematical model takes the following form:

$$\begin{aligned} X = {} & X_0 + X_{\dot{u}}\dot{u} + X_u(\Delta u) + X_{uu}(\Delta u)^2 + X_{uuu}(\Delta u)^3 + X_{vv}v^2 + X_{rr}r^2 \\ & + X_{\delta\delta}\delta^2 + X_{vvu}v^2(\Delta u) + X_{rru}r^2(\Delta u) + X_{\delta\delta u}\delta^2(\Delta u) + X_{vr}vr \\ & + X_{v\delta}v\delta + X_{r\delta}r\delta + X_{vru}vr(\Delta u) + X_{v\delta u}v\delta(\Delta u) + X_{r\delta u}r\delta(\Delta u) \end{aligned} \tag{2.10a}$$

$$\begin{aligned} Y = {} & Y_0 + Y_u(\Delta u) + Y_{uu}(\Delta u)^2 + Y_{uuu}(\Delta u)^3 + Y_{\dot{v}}\dot{v} + Y_v v + Y_{vv}v^2 \\ & + Y_{vvv}v^3 + Y_{vrr}vr^2 + Y_{v\delta\delta}v\delta^2 + Y_{vu}v(\Delta u) + Y_{vuu}v(\Delta u)^2 \\ & + Y_{\dot{r}}\dot{r} + Y_r r + Y_{rrr}r^3 + Y_{rvv}rv^2 + Y_{r\delta\delta}r\delta^2 + Y_{ru}r(\Delta u) \\ & + Y_{ruu}r(\Delta u)^2 + Y_\delta\delta + Y_{\delta\delta\delta}\delta^3 + Y_{\delta vv}\delta v^2 + Y_{\delta rr}\delta r^2 \\ & + Y_{\delta u}\delta(\Delta u) + Y_{\delta uu}\delta(\Delta u)^2 + Y_{\delta\delta\delta u}\delta^3(\Delta u) + Y_{vr\delta}vr\delta \end{aligned} \tag{2.10b}$$

$$
\begin{aligned}
N = {} & N_0 + N_u(\Delta u) + N_{uu}(\Delta u)^2 + N_{uuu}(\Delta u)^3 + N_{\dot{v}}\dot{v} + N_v v + N_{vv}v^2 \\
& + N_{vvv}v^3 + N_{vrr}vr^2 + N_{v\delta\delta}v\delta^2 + N_{vu}v(\Delta u) + N_{vuu}v(\Delta u)^2 \\
& + N_{\dot{r}}\dot{r} + N_r r + N_{rrr}r^3 + N_{rvv}rv^2 + N_{r\delta\delta}r\delta^2 + N_{ru}r(\Delta u) \\
& + N_{ruu}r(\Delta u)^2 + N_\delta \delta + N_{\delta\delta\delta}\delta^3 + N_{\delta vv}\delta v^2 + N_{\delta rr}\delta r^2 \\
& + N_{\delta u}\delta(\Delta u) + N_{\delta uu}\delta(\Delta u)^2 + N_{\delta\delta\delta u}\delta^3(\Delta u) + N_{vr\delta}vr\delta
\end{aligned}
\tag{2.10c}
$$

where $\Delta u = u - V$ is the disturbance in surge velocity. The coefficients in equation (2.10) are written according to simplified derivative notation of SNAME (Nomenclature, 1952). Each coefficient represents a term in the Taylor Series expansion, e.g.,

$$
X_{uu} = \frac{1}{2}\frac{\partial^2 X}{\partial(\Delta u)^2} \ , \qquad X_{v\delta} = \frac{\partial^2 X}{\partial\delta\,\partial v} \ .
$$

To mention briefly, another mathematical model to represent the hydrodynamic forces and moments was proposed by the Japanese Mathematical Modeling Group, JMMG, in the late 1970s last century. In this expression the hydrodynamic forces and moments are separated into several parts, such as; acting on the ship hull, the propeller and rudder, respectively, in the following form:

$$
X = X_H + X_P + X_R \tag{2.11a}
$$

$$
Y = Y_H + Y_P + Y_R \tag{2.11b}
$$

$$
N = N_H + N_P + N_R \tag{2.11c}
$$

where the subscripts “H”, “P” and “R” denote the hull, the propeller and the rudder, respectively. Substituting equation (2.11) into equation (2.7), yields the equations of ship maneuvering motion. This kind of equations is called MMG model, or moduler model (Yasukawa and Yoshimura, 2015). The forces and moments are generally calculated by using empirical and/or theoretical formulas (Kijima et al., 1993).

2.5 Linear Equations of Ship Maneuvering Motion

In the Abkowitz’s mathematical model, Taylor series expansion involves higher order terms. If the only linearized terms of the Taylor expansion are considered and higher order terms are removed from the equation, consequently, linearized equations of ship maneuvering motion without a rudder effect will take form as:

$$\Delta\left(\dot{u}-v\dot{\psi}\right)=X_0+\frac{\partial X}{\partial u}\left(u-V\right)+\frac{\partial X}{\partial v}v+\frac{\partial X}{\partial r}r+\frac{\partial X}{\partial \dot{u}}\dot{u}+\frac{\partial X}{\partial \dot{v}}\dot{v}+\frac{\partial X}{\partial \dot{r}}\dot{r} \tag{2.12a}$$

$$\Delta\left(\dot{v}+u\dot{\psi}\right)=Y_0+\frac{\partial Y}{\partial u}\left(u-V\right)+\frac{\partial Y}{\partial v}v+\frac{\partial Y}{\partial r}r+\frac{\partial Y}{\partial \dot{u}}\dot{u}+\frac{\partial Y}{\partial \dot{v}}\dot{v}+\frac{\partial Y}{\partial \dot{r}}\dot{r} \tag{2.12b}$$

$$I_Z\ddot{\psi}=N_0+\frac{\partial N}{\partial u}\left(u-V\right)+\frac{\partial N}{\partial v}v+\frac{\partial N}{\partial r}r+\frac{\partial N}{\partial \dot{u}}\dot{u}+\frac{\partial N}{\partial \dot{v}}\dot{v}+\frac{\partial N}{\partial \dot{r}}\dot{r} \tag{2.12c}$$

Since the initial equilibrium condition is straight-line motion at constant speed, as described in the Abkowitz's mathematical model, there can be no Y-force acting on the ship, and considering the xz- symmetry; X_v, $X_{\dot{v}}$, X_r, $X_{\dot{r}}$, Y_u, $Y_{\dot{u}}$, N_u, $N_{\dot{u}}$ derivatives are zero.

Using the notation of SNAME mentioned before and organizing equation (2.12), the linear equations of ship maneuvering motion with moving reference frame in the horizontal plane are:

$$-X_u(u-V)+(\Delta-X_{\dot{u}})\dot{u}=0 \tag{2.13a}$$

$$-Y_v v+(\Delta-Y_{\dot{v}})\dot{v}-(Y_r-\Delta V)r-Y_{\dot{r}}\dot{r}=0 \tag{2.13b}$$

$$-N_v v-N_{\dot{v}}\dot{v}-N_r r+(I_z-N_{\dot{r}})\dot{r}=0 \tag{2.13c}$$

2.5.1 Non-dimensionalization

In order to generalize the problem and to ease studying influence of parameters, it is convenient to nondimensionalize the equation (2.13). The procedure follows the prime system of SNAME (Nomenclature, 1952). According to this system, L, L/V and $\frac{1}{2}\rho L^2T$ are used as the dimensions for length, time and mass, respectively, where L is the ship advance speed, ρ is the water density and T is the draft of the ship. Then, some of the nondimensional parameters are given below:

$$\Delta'=\frac{\Delta}{\frac{1}{2}\rho L^3};\qquad (\Delta u)'=\frac{u-V}{V}=u'-1;\qquad \dot{v}'=\frac{\dot{v}L}{V^2};$$

$$\dot{r}'=\frac{\dot{r}L^2}{V^2};\qquad X'=\frac{X}{\frac{1}{2}\rho V^2LT};\qquad N'=\frac{N}{\frac{1}{2}\rho V^2L^2T}; \tag{2.14}$$

$$Y_v'=\frac{Y_v}{\frac{1}{2}\rho VLT};\qquad N_r'=\frac{N_r}{\frac{1}{2}\rho VL^3T};\qquad N_{\dot{r}}'=\frac{N_{\dot{r}}}{\frac{1}{2}\rho L^4T}.$$

2.5.2 Control forces and moments

Repeating the nondimensionalization procedure for related terms and neglecting the surge equation, equation (2.13) becomes in nondimensional form:

$$-Y'_v v' + (\Delta' - Y'_{\dot{v}})\dot{v}' - (Y'_r - \Delta')r' - Y'_{\dot{r}}\dot{r}' = 0 \tag{2.15a}$$

$$-N'_v v' - N'_{\dot{v}}\dot{v}' - N'_r r' + (I'_z - N'_{\dot{r}})\dot{r}' = 0 \tag{2.15b}$$

In the linearized equations of motion, it should not be overlooked that all of the terms must include the effect of the ship's rudder held at zero degrees (on the centreline). Considering the effect of controls working on the path of a ship, on the other hand, must include terms that express the control forces and moments created by rudder deflection or any other control devices as functions of time (Lewis, 1989).

The rudder deflection creates two linearized components acting at the center of gravity of the ship. The first one is y-component denoted by $Y_\delta\delta$ and the second one is the moment created about the z-axis of the ship and denoted by $N_\delta\delta$.

There are some restrictions for the case of small perturbations, such as Y_v, N_v, Y_r and N_r which are evaluated at $\delta = 0$ assumed not to change at any rudder deflection and for usual ship configurations $Y_{\dot{r}} \approx 0$ and $N_{\dot{r}} \approx 0$. Including the rudder force and moment, the equations of motion become as follows:

$$n'_z \dot{r}' - N'_v v' - N'_r r' = N'_\delta \delta \tag{2.16a}$$

$$\Delta'_y \dot{v}' - Y'_v v' - (Y'_r - \Delta) r' = Y'_\delta \delta \tag{2.16b}$$

where

$$n'_z = I'_z - N'_{\dot{r}} \cong 2I'_z$$

$$\Delta'_y = \Delta' - Y'_{\dot{v}} \cong 2\Delta'$$

2.5.3 Motion stability of a ship

Motion stability of a ship is associated with coursekeeping or stability of direction. Assume that a vessel is in a stable condition, until an external force or moment disturb it for an instant. After the disturbance factor released from the vessel, it tends to return to the state of equilibrium existing before the body was disturbed. What is desired for

motion stability of a ship is to return the original path after the disturbance factor is cleared, without any intervention by the helmsman or automatic control (Lewis, 1989)

There are various kinds of motion stability associated with ships (Arentzen, 1960):

a. Straight-line stability (so-called dynamic stability)

b. Directional stability

c. Positional motion stability.

Before describing all cases of motion stability, assume that the ship is initially traveling at constant speed along a straight course.

a. In the straight-line stability, the final path, after the disturbance factor disappears, is also a straight-line but in a different direction of the first one.

b. Directional stability is divided into two different types. In the first type, the final path has the same direction and possess straight-line as well as the first one but in a different transverse position. The second one is the same as the first but the ship doesn't oscillate under the thumb of disturbance factor.

c. Positional motion stability may be the ideal stability for a ship that the ship not only returns to its original path and possess straight-line but also has the same transverse position relative to the surface of the earth.

Case b and c are more complicated that it is not possible for a ship to have these kinds of motion stabilities without various degrees of automatic control. However, achieving straight-line stability (case a) is more feasible for most ships which are steered manually.

2.5.4 Controls-fixed stability

The equation (2.16) consists of two simultaneous differential equations of the first order in two unknowns, the sway velocity v' and the yaw angular velocity r'. The simultaneous solution of these two equations provide a stability criterion, which is denoted by C, given below:

$$C = Y'_v N'_r - N'_v (Y'_r - \Delta) \tag{2.17}$$

For the positive values of C, the ship is considered to have dynamic course stability. Otherwise, it does not have.

2.6 Physical Interpretation of Hydrodynamic Derivatives

Hydrodynamic derivatives are the change of hydrodynamic forces and moments according to independent variables, such as u, v, δ and $\dot{u}$. Besides the value, the sign of hydrodynamic derivatives are also important to define the characteristics. In order to understand the physical meaning of hydrodynamic derivatives, e.g., linear derivatives are treated.

Firstly, the derivative $Y_{\dot{v}}$ will be considered. The mathematical definition is the rate of change of Y-force with respect to acceleration $\dot{v}$. In this condition, bow and stern will be accelerated in the same direction, hence the inertial reaction forces will occure in the negative y-direction. As a result, derivative $Y_{\dot{v}}$ will always have a negative value. For ship-shaped bodies with large length to beam (L/B) ratios, the magnitude of this derivative is approximately equal to the ship's displacement. In the same way, $N_{\dot{r}}$ is also always negative and has a large value approximately as I_z.

In the case of $Y_{\dot{r}}$ and $N_{\dot{v}}$, bow and stern reacting oppositely. Therefore, these derivatives have a relatively small values of uncertain sign.

Derivative Y_v has always negative value in a similar manner of $Y_{\dot{v}}$. For derivative N_v whether having a rudder has a great importance. This derivative has usually negative value for ships without fins or rudders at the stern. However, if a rudder exists and located at the stern of the ship, it will decrease the negativity of N_v.

The effect of an angular velocity r on Y and N is that a positive r causes to a large negative N_r. On the other hand, positive r causes to a small positive or negative Y-force (Y_r). If the bow dominates, Y_r has a negative value.

2.7 Determination of Hydrodynamic Derivatives

Hydrodynamic derivatives are determined from the captive model tests (ITTC, 2002). The harmonic derivatives are calculated from the pure sway, pure yaw and yaw and drift data. Derivatives such as X_0, X_{vv}, X_{rr}, $X_{\delta\delta u}$, Y_δ, $Y_{\delta\delta\delta}$, N_δ and $N_{\delta u}$ are calculated from the static speed, static rudder, static drift and rudder and drift CFD simulations. When the rate of change of X-force versus v is plotted and fitted by

using a curve of 3^{rd}-degree, then only the even powers of v will be considered and the odd powers must be zero. This is also adopted for $\dot{v}, r, \dot{r}$ and δ. As a result, X is an even function of this variables, e.g.:

$$X(v) = a_0 + a_2 v^2 + a_4 v^4 + a_6 v^6 + \ldots \quad (2.18a)$$

$$X(\dot{v}) = a_0 + a_2 \dot{v}^2 + a_4 \dot{v}^4 + a_6 \dot{v}^6 + \ldots \quad (2.18b)$$

$$X(\delta) = a_0 + a_2 \delta^2 + a_4 \delta^4 + a_6 \delta^6 + \ldots \quad (2.18c)$$

The coefficients denoted by a_n represents each term of Abkowitz's Taylor Series expansion, e.g., in equation (2.18a) $a_2 = \frac{1}{2} X_{vv}$. The point to be noted here is that the a_n calculated from the functions represents the hydrodynamic derivative multiplied by Taylor Series coefficients. The expression of Abkowitz's mathematical model also has the same manner for simplicity.

The expressions of Y and N functions differ from X, in such a way that Y and N are odd functions of the variables mentions above, e.g.:

$$Y(v) = a_0 + a_1 v^1 + a_3 v^3 + a_5 v^5 + \ldots \quad (2.19a)$$

$$Y(\delta) = a_0 + a_1 \delta^1 + a_3 \delta^3 + a_5 \delta^5 + \ldots \quad (2.19b)$$

3. URANS METHOD

It is crucial to estimate the hydrodynamic performance of a floating vessel numerically or experimentally. As is known, the experimental methods are expensive and time consuming. Also there are several uncertainties caused by the experimental measurement equipments. Meanwhile, numerical methods are cost effective as compared with the experiments and are quick-responding methods. In addition to this, CFD method can be employed for both simulating inviscid and viscous flows. These methods have been used in order to calculate the hydrodynamic forces and moments acting on the ship.

As mentioned in Chapter 1, viscous effects play a significant role in ship maneuvering motions. Starting from this point of view, well known computational fluid dynamics (CFD) technique based on finite volume method (FVM) is preferred instead of the empirical/semi-empirical approaches and theoretical calculations.

This chapter is divided into six sub-sections. In the first sub-section, the URANS method will be introduced. In the second sub-section turbulence models will take part. Then, the finite volume discretization technique will be explained. The Volume of Fluid (VOF) method will follow and pressure and velocity coupling technique will be presented right after. Finally, the solution methodology will be given.

3.1 Reynolds-averaged Navier-Stokes (RANS) Equations

A fluid element considered in a fluid motion must satisfy the conservation laws which are governing all natural phenomena, given below:

- Conservation of mass
- Conservation of momentum
- Conservation of energy

Each law is represented with a spesific formula called governing equation. The continuity equation for the mass conservation and the Navier-Stokes equations for the conservation of

momentum, govern the 3D motion of the incompressible and viscous fluid. Continuity equation can be represented by the following equation:

$$\frac{D\rho}{Dt} + \rho \nabla . V = 0 \tag{3.1}$$

The open form of continuity equation:

$$\frac{\partial \rho}{\partial t} + V . \nabla \rho + \rho \nabla . V = \frac{\partial \rho}{\partial t} + \nabla . (\rho V) = 0 \tag{3.2}$$

The viscous flow calculations have been made assuming that the flow is 3D, incompressible, transient and fully turbulent. For an incompressible flow, the rate of change of density ρ with respect to time must be zero, i.e., $\rho = const$. This condition leads us to reduce continuity equation to the following statement for incompressible fluid flow:

$$\nabla . V = 0 \tag{3.3}$$

Navier-Stokes equations are given as follows:

$$\begin{aligned} \rho \frac{Du}{Dt} = \rho f_x - \frac{\partial p}{\partial x} + \frac{\partial}{\partial x}\left[\mu \left(-\frac{2}{3} \nabla . V + 2 \frac{\partial u}{\partial x} \right) \right] \\ + \frac{\partial}{\partial y}\left[\mu \left(\frac{\partial v}{\partial x} + \frac{\partial u}{\partial y} \right) \right] + \frac{\partial}{\partial z}\left[\mu \left(\frac{\partial \omega}{\partial x} + \frac{\partial u}{\partial z} \right) \right] \end{aligned} \tag{3.4a}$$

$$\begin{aligned} \rho \frac{Dv}{Dt} = \rho f_y - \frac{\partial p}{\partial y} + \frac{\partial}{\partial y}\left[\mu \left(-\frac{2}{3} \nabla . V + 2 \frac{\partial v}{\partial y} \right) \right] \\ + \frac{\partial}{\partial x}\left[\mu \left(\frac{\partial v}{\partial x} + \frac{\partial u}{\partial y} \right) \right] + \frac{\partial}{\partial z}\left[\mu \left(\frac{\partial \omega}{\partial y} + \frac{\partial v}{\partial z} \right) \right] \end{aligned} \tag{3.4b}$$

$$\begin{aligned} \rho \frac{D\omega}{Dt} = \rho f_z - \frac{\partial p}{\partial z} + \frac{\partial}{\partial z}\left[\mu \left(-\frac{2}{3} \nabla . V + 2 \frac{\partial \omega}{\partial z} \right) \right] \\ + \frac{\partial}{\partial x}\left[\mu \left(\frac{\partial \omega}{\partial x} + \frac{\partial u}{\partial z} \right) \right] + \frac{\partial}{\partial y}\left[\mu \left(\frac{\partial \omega}{\partial y} + \frac{\partial v}{\partial z} \right) \right] \end{aligned} \tag{3.4c}$$

Considering the flow is incompressible with constant viscosity, Navier-Stokes equations can be represented with a closed formula:

$$\rho \frac{DV}{Dt} = -\nabla p + \mu \nabla^2 V + \rho f \tag{3.5}$$

In CFD simulations, the problem is recast as a system of equations for mean flow quantities, such as mean velocity and pressure $\bar{u}$, $\bar{p}$, Reynolds stresses $\bar{u}_i\bar{u}_j$, instead of computing the actual state of fluid flow. The results are obtained after averaging over many realizations. This approach is called the Reynolds-averaged Navier-Stokes (RANS) method.

The RANS equations for the flow fields which are generated by applying the averaging operation to the Navier-Stokes equations, described as (Zikanov, 2010):

$$\rho\frac{\partial \bar{u}_i}{\partial t}+\rho\frac{\partial(\bar{u}_i\bar{u}_j)}{\partial x_j}=-\frac{\partial \bar{p}}{\partial x_i}+\mu\nabla^2\bar{u}_i-\frac{\partial \tau_{ij}}{\partial x_j} \quad , \qquad \frac{\partial \bar{u}_i}{\partial x_i}=0 \tag{3.6}$$

3.2 Turbulence Modeling

Solving the Reynolds-averaged Navier-Stokes equations coupled with a turbulence model is a common approach used in recent engineering problems. Generally, the turbulence models are employed when the flow is fully turbulent. The Navier-Stokes equations govern the velocity and pressure of a fluid flow. In a turbulent flow, each of these quantities are separated into a mean part $(\bar{U})$ and a fluctuating part (u'), e.g.,

$$U=\bar{U}+u' \tag{3.7}$$

where the time-averaging velocity component is defined as:

$$\bar{U}=\frac{1}{T}\int_0^T U dt \tag{3.8}$$

where T is the averaging interval. In an unsteady flow, Ferziger and Perić (2002) described the following formula instead of time averaging:

$$\bar{U}=\frac{1}{N}\sum_{n=1}^{N}\bar{U} \tag{3.9}$$

Although there are several types of RANS turbulence models, the most popular models, $k-\varepsilon$ (Jones and Launder, 1972) and $k-\omega$ are used in the presented study. These models are also called two-equation models. The main reason for the preference of two-equation models is that they demand less computer resources than the other turbulence models.

3.2.1 k-ε turbulence model

The equations of this model are the transport equations for the turbulent kinetic energy $k(x,t)$ and the rate of viscous dissipation $\varepsilon(x,t)$. The dissipation rate, ε of the energy is written as:

$$\varepsilon = \frac{k^{3/2}}{L} \tag{3.10}$$

where k is the kinetic energy of the flow and L is the length scale involved. The $k-\varepsilon$ is related to the turbulent viscosity, ν_t based on the Prandtl mixing length model:

$$\nu_t = \rho C_\mu \frac{k^2}{\varepsilon} \tag{3.11}$$

where ρ is the density of the flow and C_μ is an empirical constant obtained from the experimental data. Including this constant to the governing equations, the k equation of the standart $k-\varepsilon$ model is written as:

$$U_i \frac{\partial(\rho U_j k)}{\partial x_j} = \frac{\partial}{\partial x_j}\left(\frac{\nu_t}{\sigma_k}\frac{\partial k}{\partial x_j}\right) + \nu_t \frac{\partial U_i}{\partial x_j}\left(\frac{\partial U_i}{\partial x_j} + \frac{\partial U_j}{\partial x_j}\right)\frac{\partial U_i}{\partial x_j} - \rho\varepsilon \tag{3.12}$$

and the ε equation:

$$U_i \frac{\partial(\rho U_j \varepsilon)}{\partial x_j} = \frac{\partial}{\partial x_j}\left(\frac{\nu_t}{\sigma_\varepsilon}\frac{\partial \varepsilon}{\partial x_j}\right) + C_{\varepsilon 1}\frac{\varepsilon}{k}\nu_t \frac{\partial U_i}{\partial x_j}\left(\frac{\partial U_i}{\partial x_j} + \frac{\partial U_j}{\partial x_j}\right)\frac{\partial U_i}{\partial x_j} - \rho C_{\varepsilon 2}\frac{\varepsilon^2}{k} \tag{3.13}$$

The commonly used values of constant parameters in the equations are:

$$C_\mu = 0.09;\ C_{\varepsilon 1} = 1.44;\ C_{\varepsilon 2} = 1.92;\ \sigma_k = 1.0;\ \sigma_\varepsilon = 1.3 \tag{3.14}$$

3.2.2 k-ω SST turbulence model

The *Shear Stress Transport* (SST) $k-\omega$ model was developed as an alternative to $k-\varepsilon$ model. The main purpose in the development of this method was to resolve the lack of $k-\varepsilon$ model. Unlike the $k-\varepsilon$ model, in the SST $k-\omega$ the variable ε is replaced by the dissipation rate per unit kinetic energy ω. The k equations in the SST model are written as:

$$U_i \frac{\partial(\rho U_j k)}{\partial x_j} = \frac{\partial}{\partial x_j}\left(\frac{\nu_t}{\sigma_k}\frac{\partial k}{\partial x_j}\right) + \nu_t \frac{\partial U_i}{\partial x_j}\left(\frac{\partial U_i}{\partial x_j} + \frac{\partial U_j}{\partial x_j}\right)\frac{\partial U_i}{\partial x_j} - \rho k\omega \tag{3.15}$$

and the ω equation:

$$U_i \frac{\partial(\rho U_j \omega)}{\partial x_j} = \frac{\partial}{\partial x_j}\left(\frac{\nu_t}{\sigma_\varepsilon}\frac{\partial \omega}{\partial x_j}\right) + a\frac{\omega}{k}\nu_t \frac{\partial U_i}{\partial x_j}\left(\frac{\partial U_i}{\partial x_j} + \frac{\partial U_j}{\partial x_j}\right)\frac{\partial U_i}{\partial x_j} - \beta\rho\omega^2 \tag{3.16}$$

where:

$$\nu_t = \rho\frac{k}{\omega} \tag{3.17}$$

3.3 Finite Volume Method (FVM)

The finite volume method (FVM) is a discretization technique for partial differential equations, especially those that arise from physical conservation laws. These methods are mainly employed for the numerical solution of problems in fluid mechanics where they were introduced in the 1970s by McDonald, MacCormack, and Paullay. FVM uses a volume integral formulation of the problem with a finite partitioning set of volumes to discretize the equations. In general, the FVM involves the following steps:

1) Decomposition of the problem domain into control volumes,
2) Formulation of integral balance equations for each control volume,
3) Approximation of integrals by numerical integration,
4) Approximation of function values and derivatives by interpolation with nodal values,
5) Assembling and solution of discrete algebraic system.

3.4 Volume of Fluid (VOF) Method

The free surface flow problem is included to the CFD simulations by using Volume of Fluid (VOF) method which is utilized by Eulerian fluid approach. The VOF method developed by Hirt and Nichols (1981) is a fixed mesh technique designed for two or more fluids, where in each cell of a mesh it is necessary to use only one value for each dependent variable defining the fluid state (Fonfach, 2010).

3.5 Segregated Flow Solver

The Segregated Flow solver is usually used for incompressible and mildly compressible flows. This solver controls the solution update for the Segregated Flow model to the SIMPLE algorithm (CD-adapco, 2014). It controls two additional solvers:

- Velocity solver
- Pressure solver

The algebraic multigrid parameters and under-relaxation factors can be set for each of these solvers.

3.6 Solution Methodology

The main objective of the presented computational study is to investigate the turning maneuvering performance of a surface combatant. According to the selected mathematical model, evaluation of the hydrodynamic derivatives takes an important part since they are used directly in the mathematical model to simulate definite ship maneuvers.

The hydrodynamic derivatives are calculated from a series of numerical simulations described in Chapter 4 in detail. The derivatives arising from acceleration and angular velocity are taken from the experimental data (Yoon, 2009). The rudder terms are also calculated numerically. Then are used in the right hand side of the ship maneuvering motion equations to simulate the turning circle maneuver. The simultaneous differential equations of motion are solved and the turning maneuver is simulated (Figure 3.1). The turning performance parameters of the ship model are compared with the available experimental data, linear model and empirical formulas.

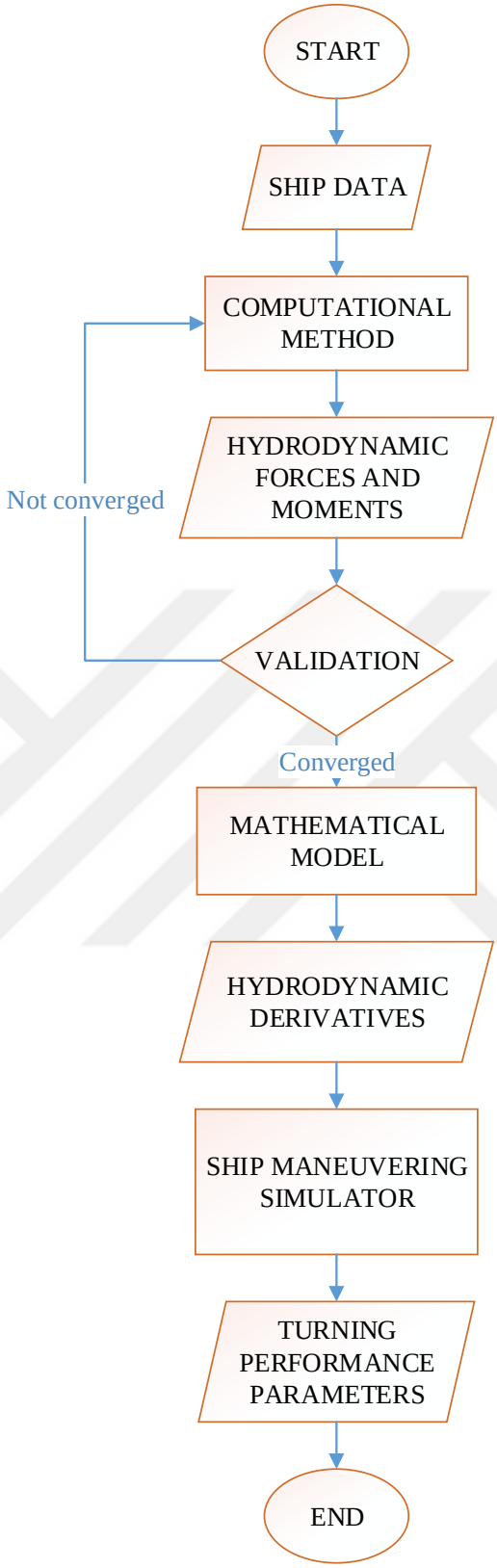

Figure 3.1 : Simulation of turning maneuver.

4. COMPUTATIONAL RESULTS

It is crucial to compare the CFD simulation results with EFD validation data in terms of accuracy of the study. In this chapter, numerical results are presented in an orderly manner. Firstly, the grid independence study is introduced. Secondly, the effect of turbulence model choice is presented. Then, hydrodynamic forces and moments take place in comparison with EFD validation data. The viscous and inviscid analyses results are also presented. Free surface deformations are examined afterwards. The hydrodynamic derivatives obtained from numerical analyses follow. Finally, the turning maneuver simulation results are presented in comparison with available validation data.

4.1 Numerical Model

As previously mentioned, the computational fluid dynamics (CFD) method is used to determine the hydrodynamic derivatives of DTMB model 5415. In this sub-section, the numerical model is described in detail. Firstly, the geometric properties of the ship model take place. The description of the problem and appropriate numerical setup is given next. The simulation matrix is presented. The computational domain and grid topology where the numerical analyses were done, are defined. Boundary conditions that are given to identify the physical conditions at the boundaries of computational domain take part.

4.1.1 Ship model geometry

The prefered model used in this study is DTMB 5512, a length of L=3.048 m and a geosim of DTMB 5415 for the US Navy DDG51. The model is un-appended except for port and starboard bilge keels, i.e., not equipped with shaft, struts, propellers, or rudders Figure 4.1.

The ship speed is 20 knots (10.456 m/s) and so the model speed is 2.929 knots (1.531 m/s). The CFD simulations were performed for Fn=0.280 condition. Principal particulars of DTMB model 5512 is given in Table 4.1 (SIMMAN, 2014).

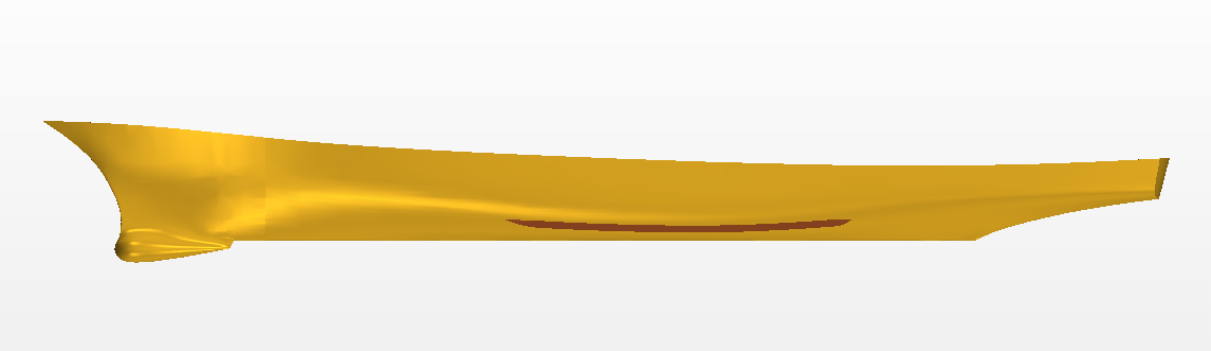

Figure 4.1 : DTMB 5415 geometry.

4.1.2 Simulation cases

It is appropriate to introduce the CFD simulation cases before giving the numerical setup. Standart PMM tests consist of both static and dynamic captive model tests (Gertler, 1967). To predict the turning maneuver characteristics of a surface combatant, a series of static PMM model tests are performed. These tests are static drift, static rudder and drift and rudder. In static drift tests, drift angle is changed from 0 to 20 degrees (Table 4.2).

Table 4.1 : DTMB model properties.

Main Particulars	Full Scale	IIHR model
L_{BP} (m)	142	3.048
L_{WL} (m)	142.18	3.052
B_{WL} (m)	19.06	0.409
B_M (m)	20	0.429
T (m)	6.15	0.132
∇ (m^3)	8424.4	0.084
C_B	0.507	0.507
C_M	0.821	0.821
S (m^2)	2972.6	1.37
Fn	0.28	0.28

Similarly, in static rudder tests, rudder angle is switched from 0 to 35 degrees but drift angle is fixed at 0 degree (Table 4.3). Drift and rudder tests are composed of static drift and static rudder tests, i.e., drift and rudder angles are switched parametrically (Table 4.4).

Table 4.2 : Static drift simulation cases.

Test name	Drift angle (°)	Rudder angle (°)
Static drift	0	0
	2	0
	4	0
	6	0
	9	0
	10	0
	11	0
	12	0
	16	0
	20	0

Table 4.3 : Static rudder simulation cases.

Test name	Drift angle (°)	Rudder angle (°)
Static rudder	0	0
	0	5
	0	10
	0	15
	0	20
	0	25
	0	30
	0	35

Table 4.4 : Drift and rudder simulation cases.

Test name	Drift angle (°)	Rudder angle (°)
Drift and rudder	0	0,5,10, …, 30,35
	4	0,5,10, …, 30,35
	8	0,5,10, …, 30,35
	12	0,5,10, …, 30,35
	16	0,5,10, …, 30,35

4.1.3 Grid topology and numerical setup

Static PMM tests (Table 4.2, Table 4.3 and Table 4.4) have been numerically simulated by using a commercial RANS solver in an unsteady manner. The ship model is fixed to sinkage and trim throughout the simulations as in the experiment (Yoon, 2009). The fluid flow is considered as 3D, incompressible and fully turbulent. The k-ε realizable turbulence model is selected. The free surface effect has been taken into account by including VOF method which is utilized by Eulerian fluid approach.

The computational domain and boundary conditions are illustrated in Figure 4.2. The origin of the coordinate system is the intersection point of forward perpendicular and base line. Hull surfaces are identified as non-slip walls. Front, top and bottom faces of the computational domain are defined as velocity inlets. Side faces are assigned as symmetry-planes and the back face is defined as pressure outlet. VOF waves are defined at draft T=0.132 m as calm water.

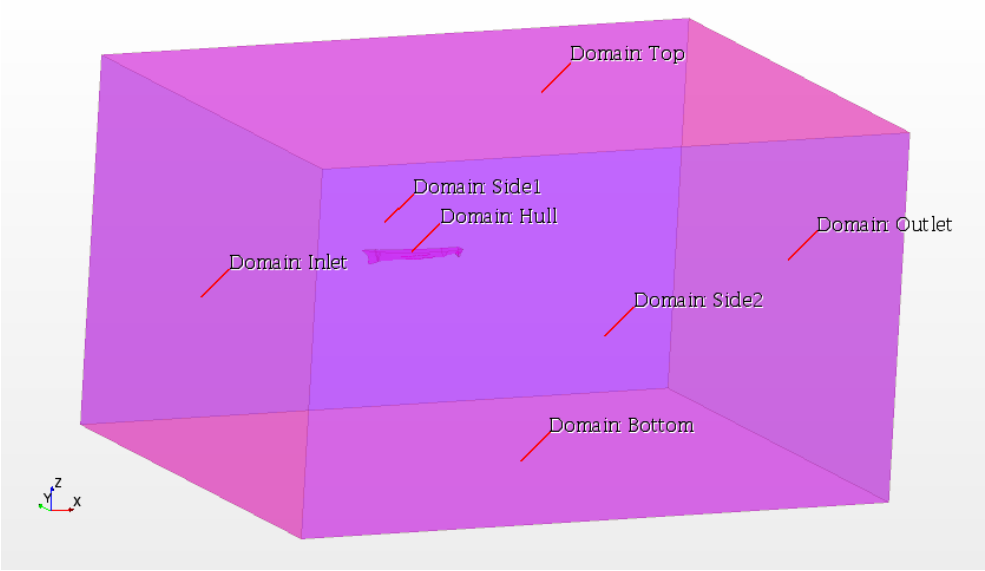

Figure 4.2 : Computational domain and boundary conditions.

The computational domain dimensions are given in Table 4.5. Upstream is in the negative and downstream is in the positive *x*-direction. The top boundary distance indicates the distance between top of domain and the origin of coordinate system.

Volumetric controls are used to refine the grid around the hull (Figure 4.3, Figure 4.4, Figure 4.5). Mesh density is increased around the free surface to capture the wave deformations well.

Table 4.5 : Computational domain dimensions.

Domain dimensions (m)			
Boundaries	Upstream	$1.8L_{BP}$	5.486
	Downstream	$3.6L_{BP}$	10.973
	Top	$1.6L_{BP}$	4.877
	Bottom	$2.1L_{BP}$	6.401
	Transverse	$2.4L_{BP}$	7.315

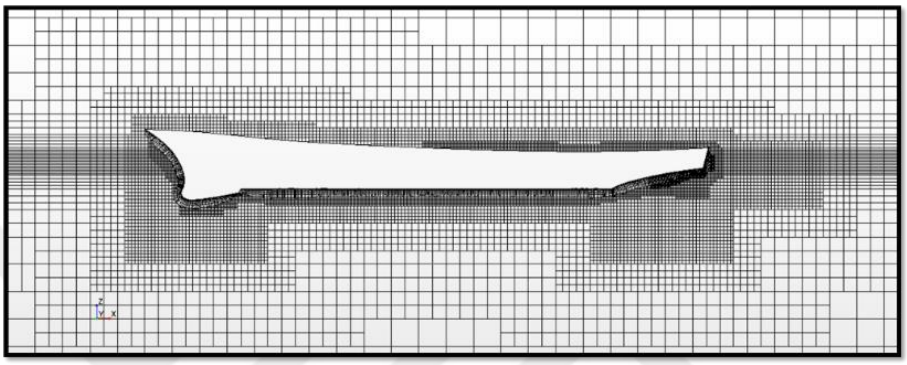

Figure 4.3 : Grid topology: profile.

It is seen that triangular mesh refinements around the free surface gives almost the same results with the rectangular ones. Considering the computational capability, triangular mesh refinements are prefered for the simulations.

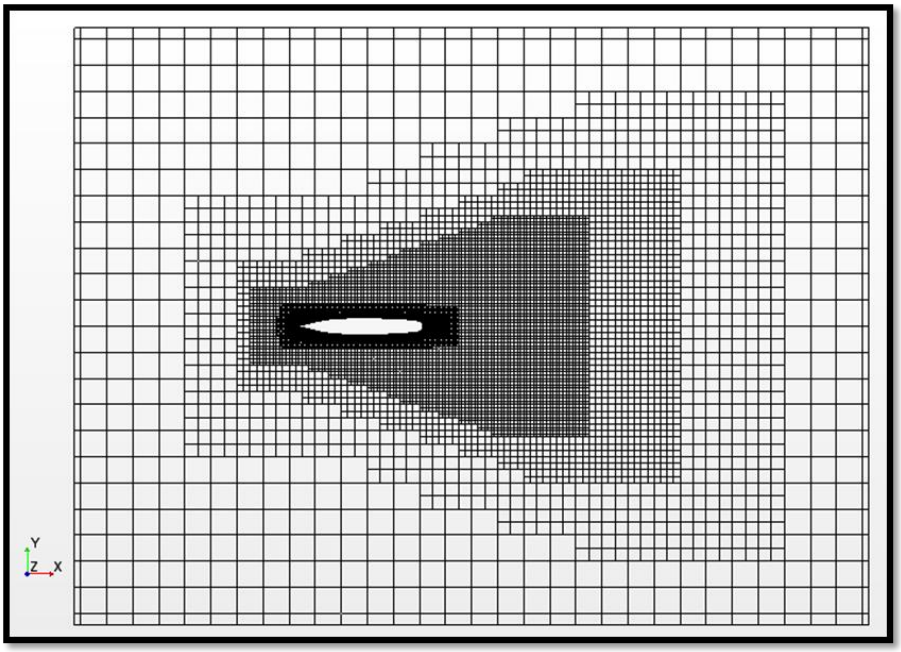

Figure 4.4 : Grid topology: top view.

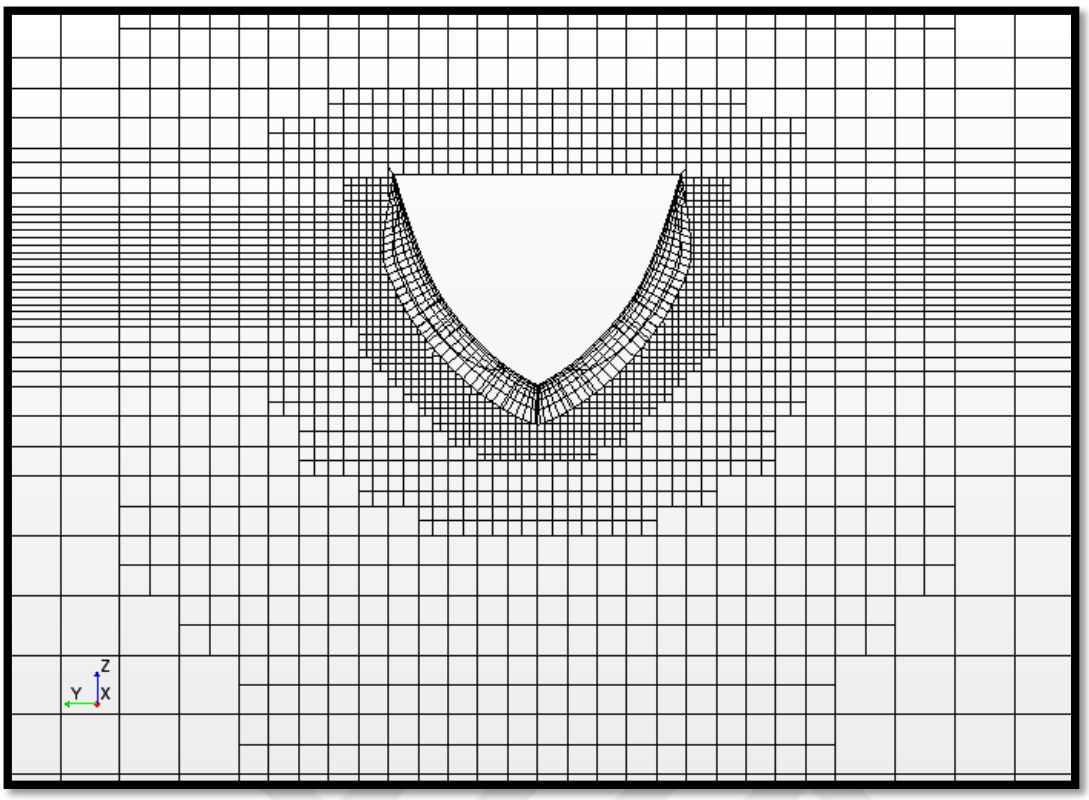

Figure 4.5 : Grid topology: x/L=0.2.

4.2 Grid Independence Study

The effects of grid quality on numerical results are investigated . For this purpose, grid independence study is performed for β=10° static drift case. The numerical simulations are repeated for different cell numbers. The finer grid is generated by multiplying base size by the square root of two and the course grid is generated by dividing base size by the square root of two. Notice that, the total number of cells doesn't take a value of the multiplication or division of two root two due to the volumetric controls. The computational results of different grid qualities are compared with the available experimental data (Yoon, 2009) and are given in Table 4.6.

Table 4.6 : Computational results of different grid qualities for 10° condition.

Grid quality	Cell Number	X'	Y'	N'	% ε_X	% ε_Y
Finer	2,363,291	0.02016	0.06092	0.02301	3.13	4.66
Fine	1,124,926	0.02050	0.06002	0.02295	4.85	6.07
Coarse	568,844	0.02082	0.05813	0.02267	6.52	9.03
Coarser	310,977	0.02151	0.05927	0.02300	10.01	7.25

Finer grid provided better results for computing forces and moments acting on the hull. If the grid quality increase, results will converge to the EFD results. Figure 4.6, Figure 4.7, Figure 4.8 and Figure 4.9 show the grid topology for each grid quality.

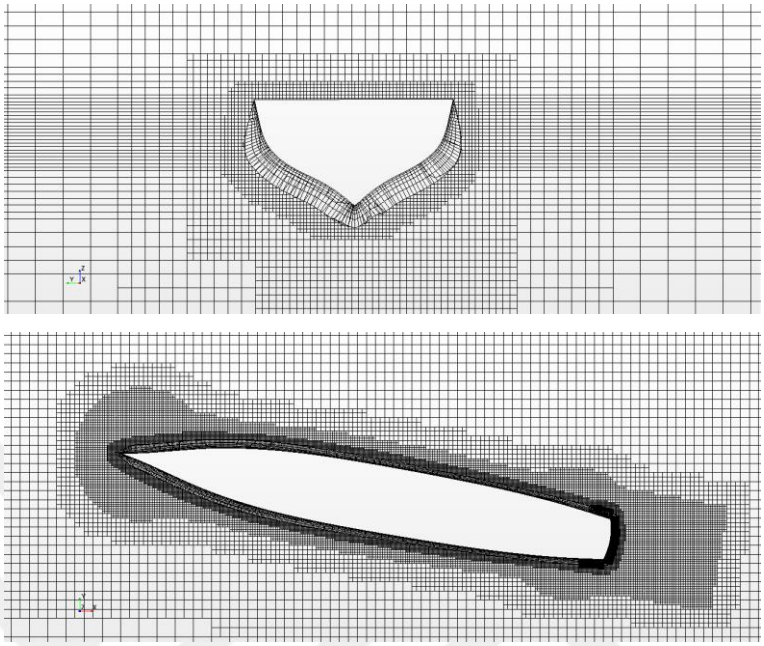

Figure 4.6 : Grid topology: finer.

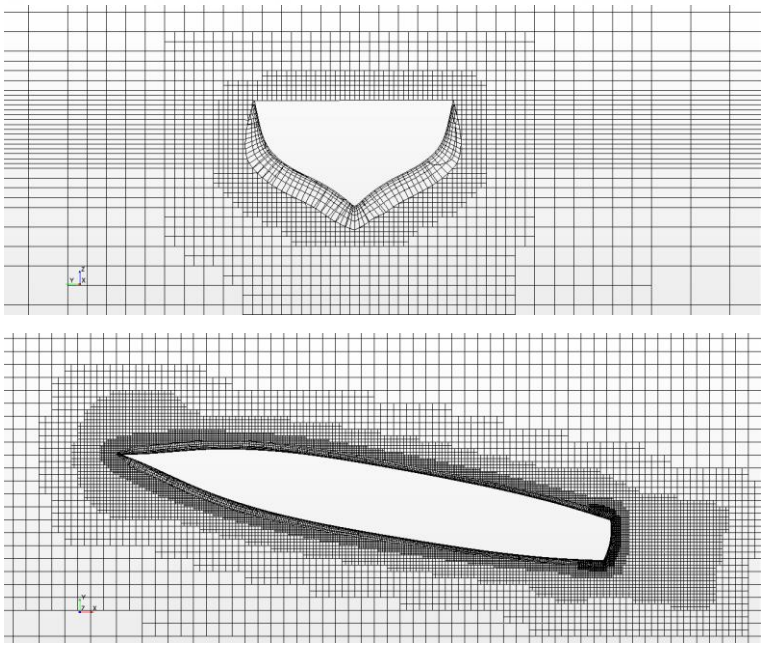

Figure 4.7 : Grid topology: fine.

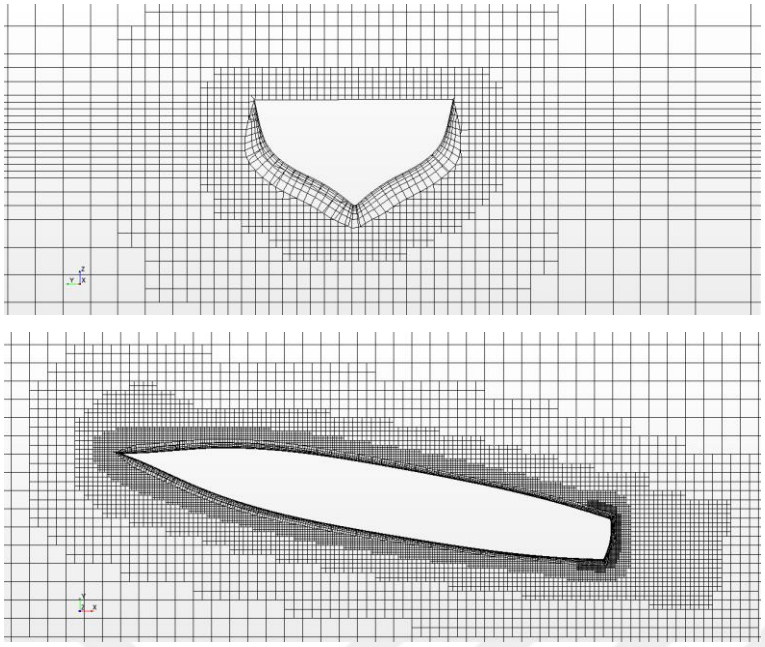

Figure 4.8 : Grid topology: coarse.

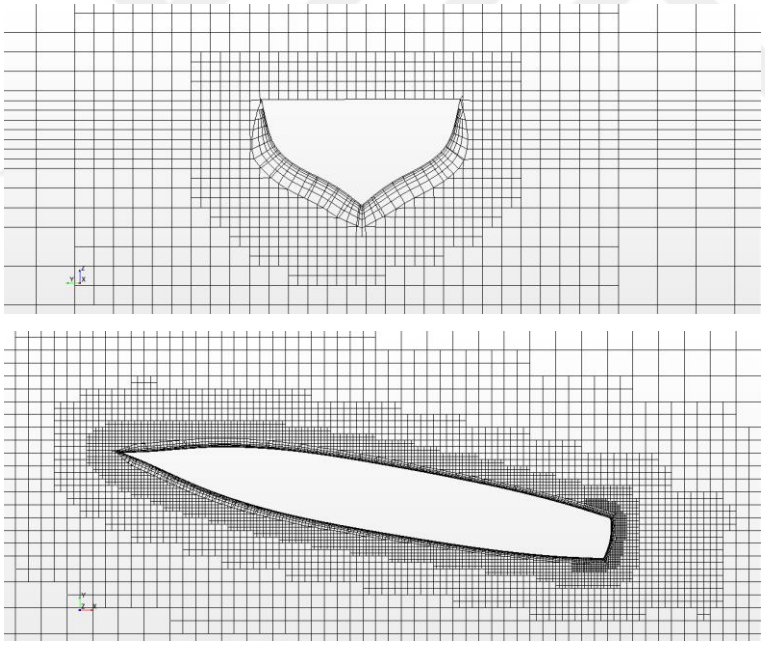

Figure 4.9 : Grid topology: coarser.

The wave profiles of each grid quality at windward side for 10° static drift condition are plotted and compared with each other (Figure 4.10).

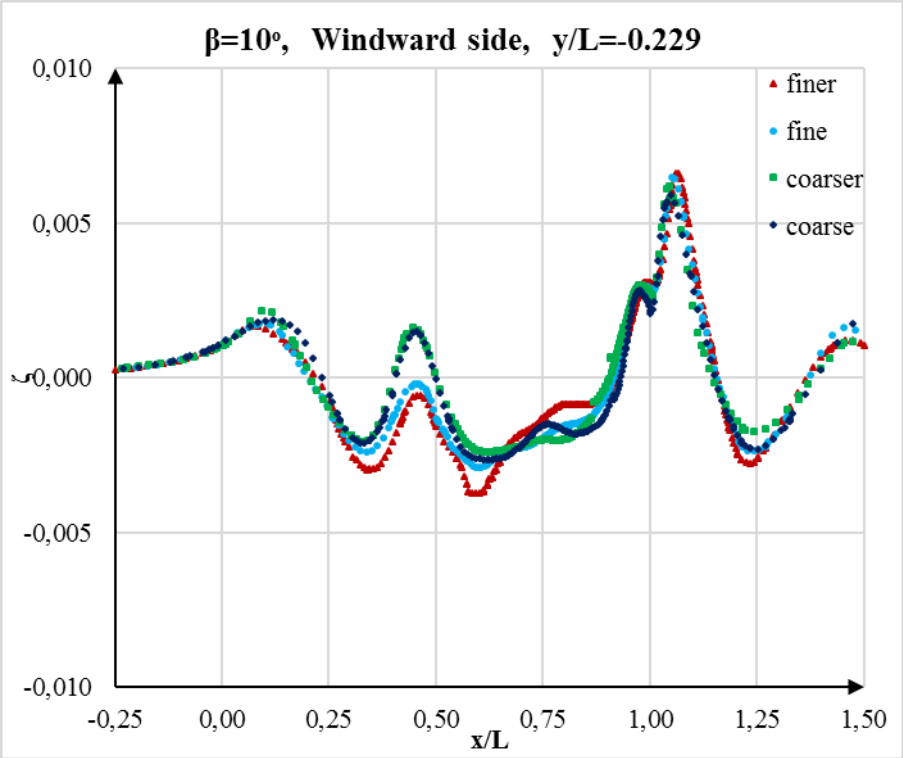

Figure 4.10 : Wave cuts of different grids at windward side for β=10°.

4.3 The Effects of Turbulence Model

The effects of turbulence model are also investigated for β=2°, β=10° and β=12° static drift cases. Two-equation models are compared with each other and with the EFD data (Table 4.7).

Table 4.7 : Comparison of two-equation turbulence models.

Static drift	Turbulence model	X'	Y'	N'	% ε_X	% ε_Y	% ε_N
β=2°	*k-ω SST*	0,01870	0,01117	0,00515	15,77	26,26	11,89
β=2°	*k-ε*	0,01822	0,01134	0,00513	12,84	28,13	11,57
β=10°	*k-ω SST*	0,02127	0,05930	0,02267	13,15	9,21	13,47
β=10°	*k-ε*	0,02050	0,06002	0,02295	9,03	10,54	12,41
β=12°	*k-ω SST*	0,02251	0,07049	0,02706	12,28	2,30	17,62
β=12°	*k-ε*	0,02163	0,07159	0,02713	7,90	0,77	17,42

Considering the overall table, the k-ε turbulence model is seem to be more suitable for the presented study. Surge forces and yaw moments are closer to the experimental data with k-ε. However, k-ω SST gives better results in the calculation of sway force at β=2° and β=10° drift angles.

4.4 Validation of Forces and Moments

Forces and moments acting on the gravity center of ship are computed for each case. The mean values of these quantities are obtained from time-averages of numerical results. The averaging operations were performed within the quasi-steady state interval.

The unappended simulation results are compared with EFD validation data (Yoon, 2009) in Table 4.8. Then the percentage of errors are given in Table 4.9. Forces and moments are given in the ship-fixed coordinate system. X', Y' and N' indicate the surge force (resistance), sway force and moment, respectively.

Table 4.8 : Comparison of computational and experimental results.

Test name	Drift angle (°)	X'	Y'	N'	X'_{EFD}	Y'_{EFD}	N'_{EFD}
Static drift	0	0.01722	0.00000	0.00000	0.01600	0.00320	0.00100
	2	0.01726	0.01124	0.00517	0.01615	0.00885	0.00460
	6	0.01812	0.03211	0.01566	0.01735	0.02870	0.01500
	9	0.01934	0.04688	0.02400	0.01845	0.04670	0.02310
	10	0.02001	0.05183	0.02664	0.01880	0.05430	0.02620
	11	0.02043	0.05754	0.02902	0.01955	0.06390	0.03000
	12	0.02122	0.06303	0.03106	0.02005	0.07215	0.03285
	16	0.02611	0.09372	0.03881	0.02385	0.10485	0.04490
	20	0.03244	0.13059	0.04650	0.02750	0.14365	0.05530

Table 4.9 : The error of computational results.

Test name	Drift angle (°)	ε_X %	ε_Y %	ε_N %
Static drift	0	7.62%	-	-
	2	6.85%	26.97%	12.48%
	6	4.43%	11.87%	4.41%
	9	4.81%	0.38%	3.89%
	10	6.42%	4.55%	1.68%
	11	4.48%	9.96%	3.26%
	12	5.86%	12.64%	5.46%
	16	9.46%	10.61%	13.56%
	20	17.96%	9.09%	15.91%

As seen in Table 4.9, computational results are agreeable with EFD data. It is observed that the percentage of error decreases with the increase of drift angle for sway forces where drift angle is less than 9°. Forces and moments obtained from numerical analyses are plotted with EFD data (Yoon, 2009) in the following figures (Figure 4.11, Figure 4.12 and Figure 4.13).

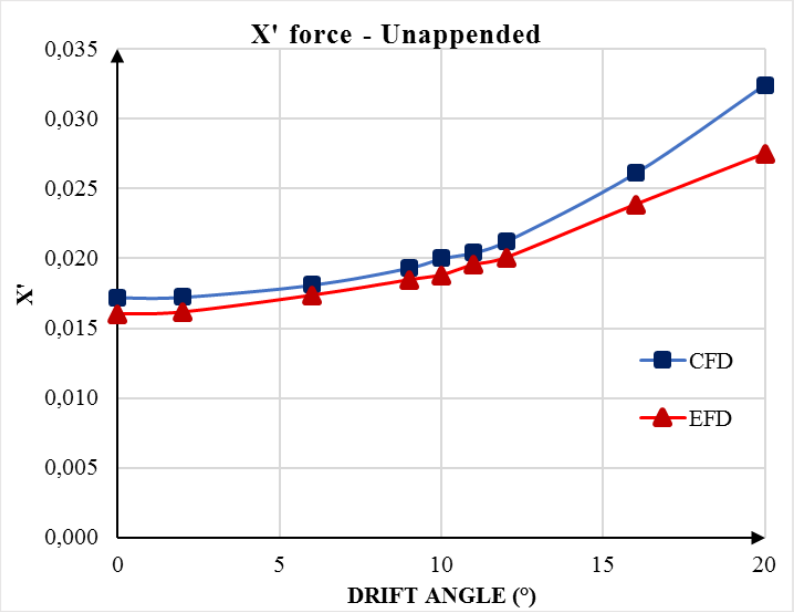

Figure 4.11 : Comparison of CFD and EFD results for X'.

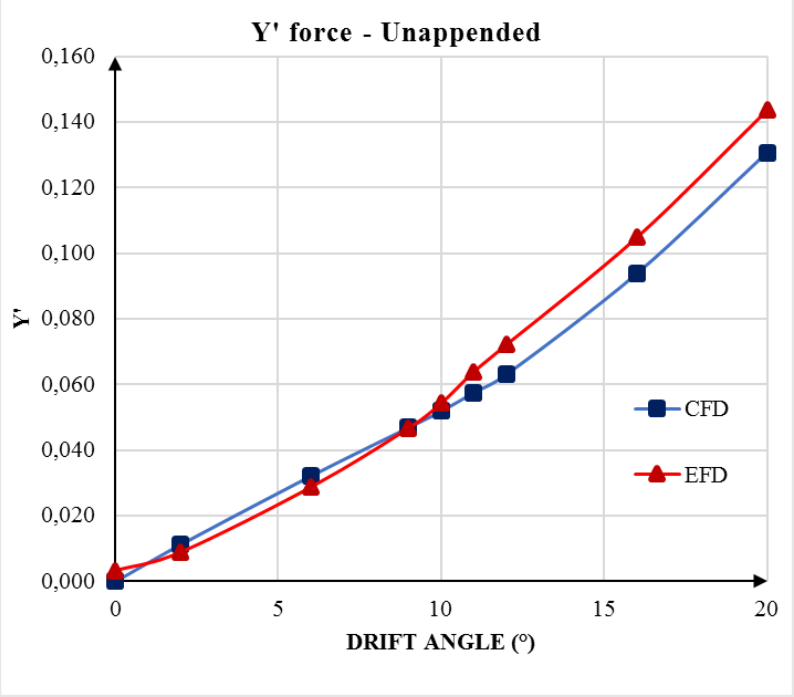

Figure 4.12 : Comparison of CFD and EFD results for Y'.

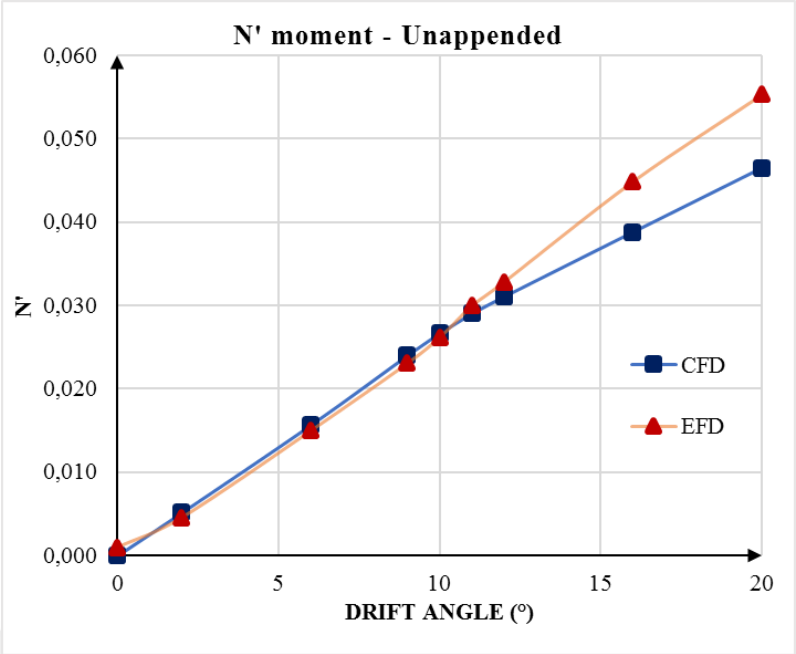

Figure 4.13 : Comparison of CFD and EFD results for N'.

Figure 4.11 shows that surge forces calculated numerically are slightly higher than the EFD results. Sway forces also show good agreement especially for drift angles lower than 11° (Figure 4.2). However, moment values increase significantly for drift angles higher than 11° (Figure 4.3).

To calculate the rudder terms, numerical simulations of appended ship model are also performed. The additional forces and moments acting on the hull due to the rudder are given in Table 4.10.

Table 4.10 : Additional forces and moments due to the rudder.

	Drift angle (°)	ΔX'	ΔY'	ΔN'
Rudder force & moment	0	0.00079	0.00000	0.00000
	2	0.00097	0.00010	-0.00004
	6	0.00077	0.00444	-0.00201
	9	0.00052	0.00730	-0.00329
	10	0.00049	0.00819	-0.00369
	11	0.00055	0.00858	-0.00381
	12	0.00041	0.00856	-0.00393
	16	0.00014	0.00950	-0.00524
	20	-0.00006	0.01220	-0.00574

Figure 4.14 and Figure 4.15 show the wall shear stress distribution on the hull and rudders for 20° static drift condition.

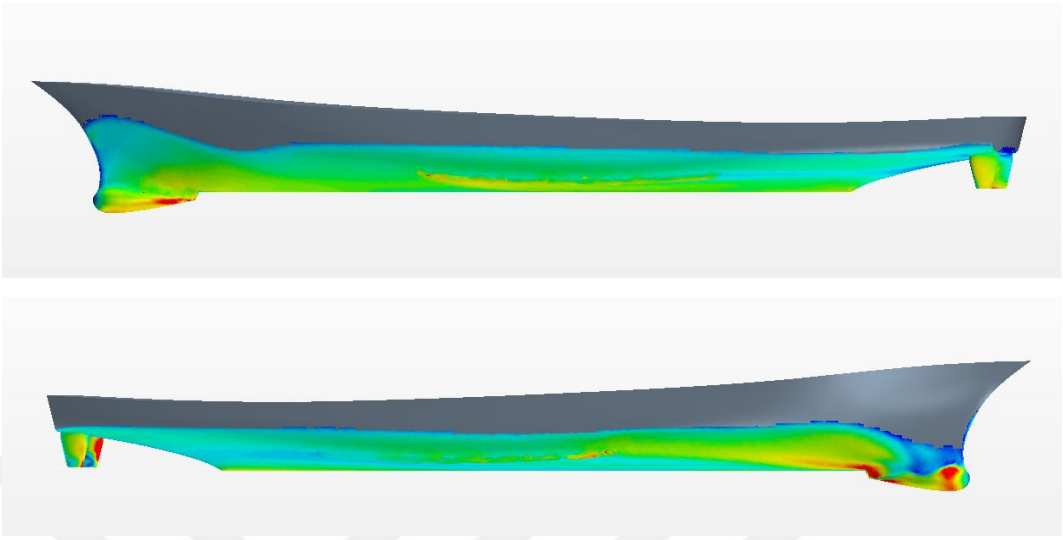

Figure 4.14 : Shear stress on the hull for β=20° condition.

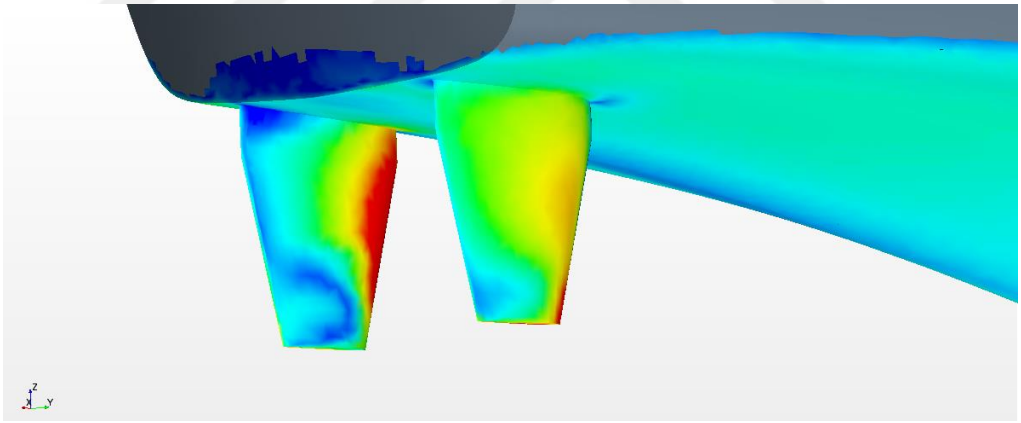

Figure 4.15 : Shear stress on the rudders with no deflection for β=20° condition.

4.5 Free Surface Deformation

As known, nonlinearities and flow separations increase with the increase of drift angle. The accuracy of the analyses at higher drift angles must be examined. Hence, free surface deformations for two different cases will be discussed in this section. These are β=0° and β=20° static drift cases.

The first case is straight-ahead condition. Free surface deformation at the symmetry plane can be seen in Figure 4.16. Deformations are observed at bow and aft. Free surface tends to rise in positive z-direction around the wake and the bow.

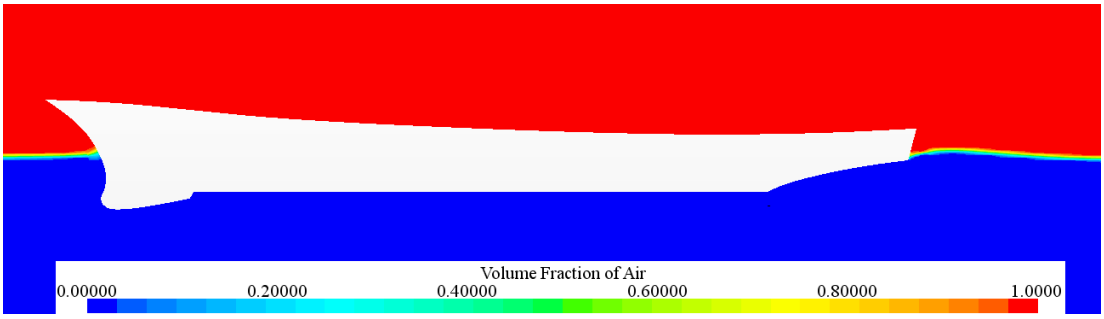

Figure 4.16 : Wave deformations at the symmetry-plane for β=0°.

The free surface wave contours are presented in Figure 4.17. Wave crests and wave troughs are formed along the ship by turns. The Kelvin waves can also be observed especially around midship and wake.

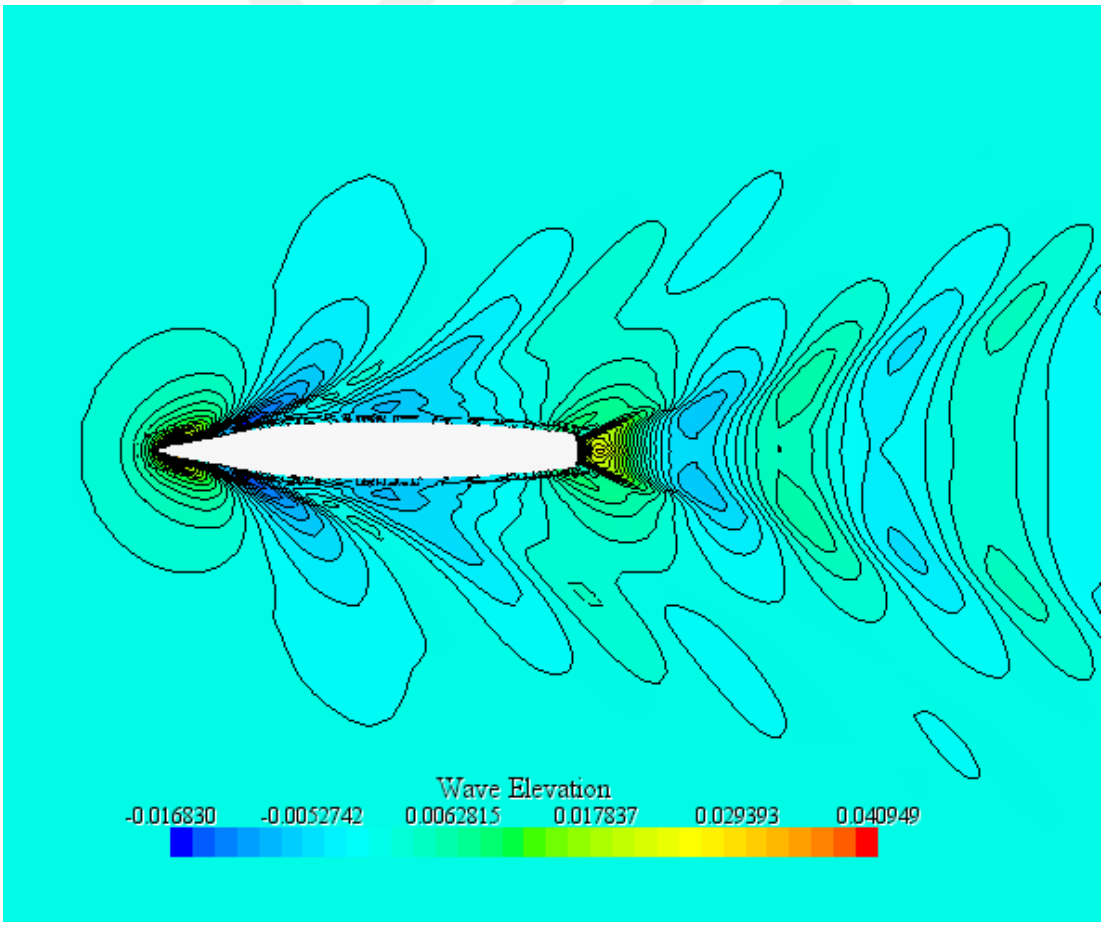

Figure 4.17 : Free surface wave contours at Fn=0.28 for β=0°.

The free surface deformations obtained from numerical analyses are compared with the EFD validation data (Longo et. al., 2005) in Figure 4.18. The *x*-axes of this figure is nondimensional ship length and *y*-axes is nondimensional transverse distance. The wave elevation scale is located in the upper right corner of the figure. In this comparison the locations of wave crest and wave trough take an important place. The general trend of free surface waves can clearly be seen to be compatible with the EFD data.

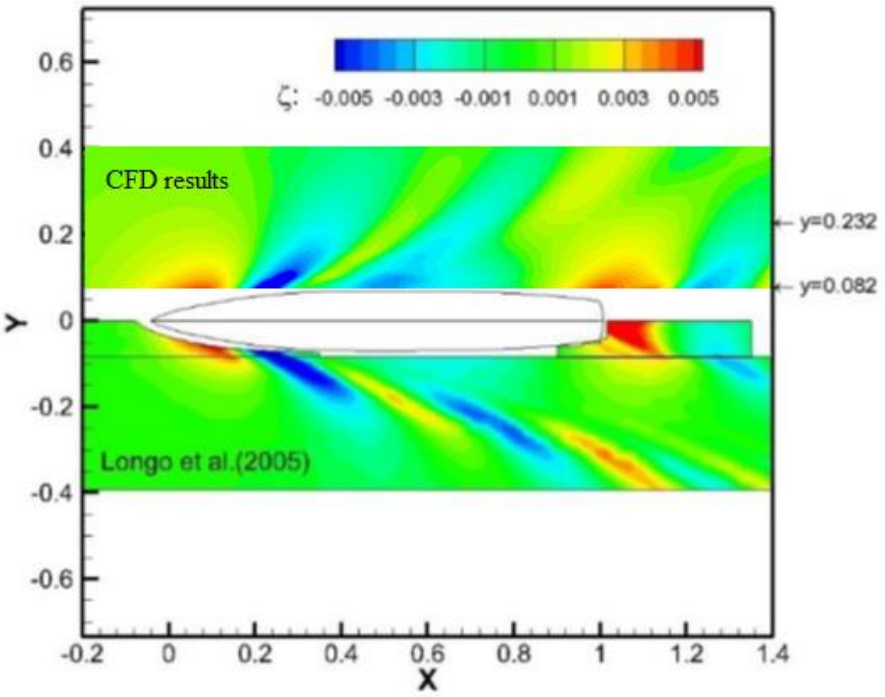

Figure 4.18 : Wave deformations for β=0° condition: CFD-top, EFD-bottom.

To make a more detailed investigation, a particular section is taken from the free surface at y/L=0.082 for 0° drift angle case. The location of this section can be seen in Figure 4.18. The wave profile on this section is plotted and compared with the EFD validation data (Bhushan et al., 2015) in Figure 4.19. The *x*-axes and *y*-axes of the wave profile figures are nondimensional *x*-position and nondimensional wave elevation, respectively. Figure A.1 illustrates the turbulent kinetic energy and Figure A.2 illustrates the vorticity magnitude on the sections taken around the ship and normal to *x*-direction.

The general characteristics of numerical results show good agreement with the EFD data. Free surface tends to rise in the front zone. Just behind the sonar dome, a wave

trough is observed in both figures. A wave crest can also be noticed around the wake where the flow is separated from the ship.

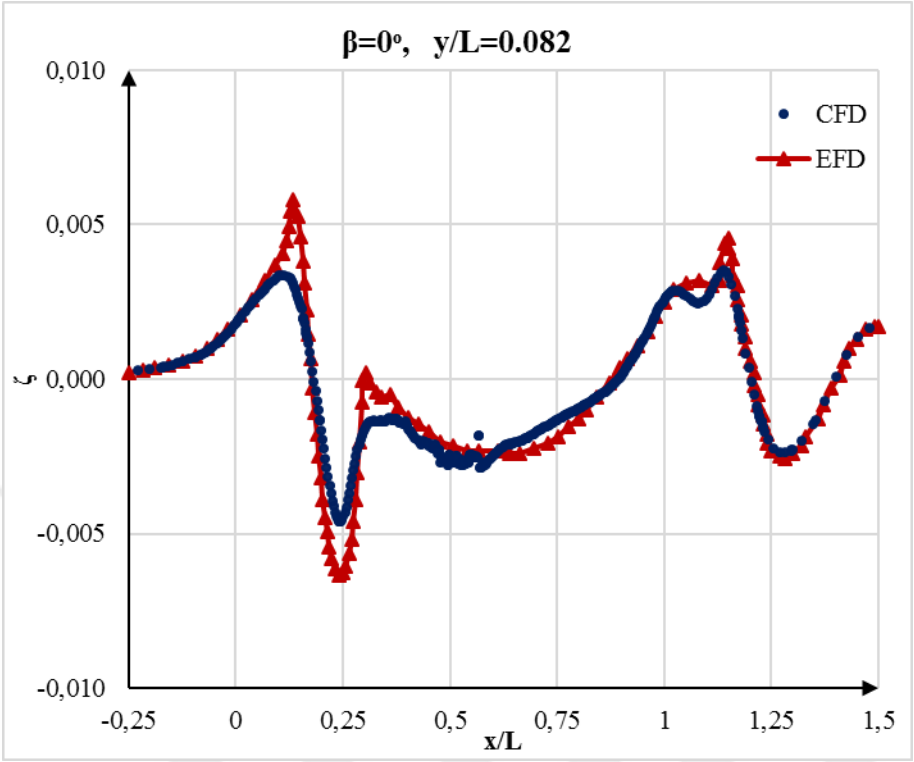

Figure 4.19 : CFD and EFD wave profiles at y/L=0.082 for β=0°.

The next case is $\beta = 20°$ static drift condition. Free surface tends to rise at the bow-port side of the ship (Figure 4.20). The flow is separated at bow (Figure 4.23) and aft and is tended to keep the initial direction.

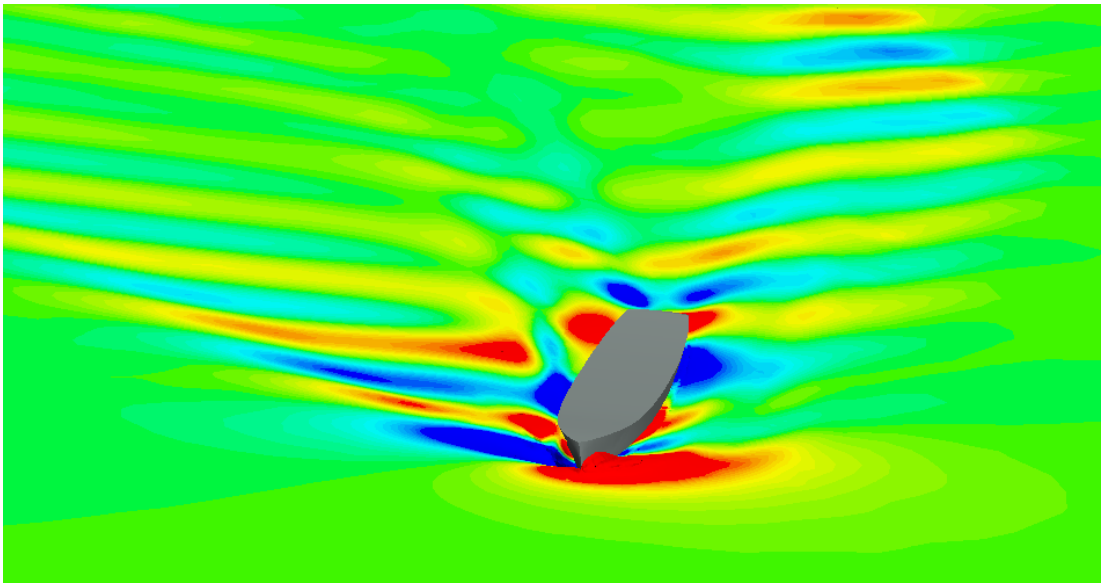

Figure 4.20 : Wave deformations for 20° condition.

Figure B.1 illustrates the turbulent kinetic energy and Figure B.2 illustrates the vorticity magnitude on the sections taken around the ship and normal to *x*-direction.

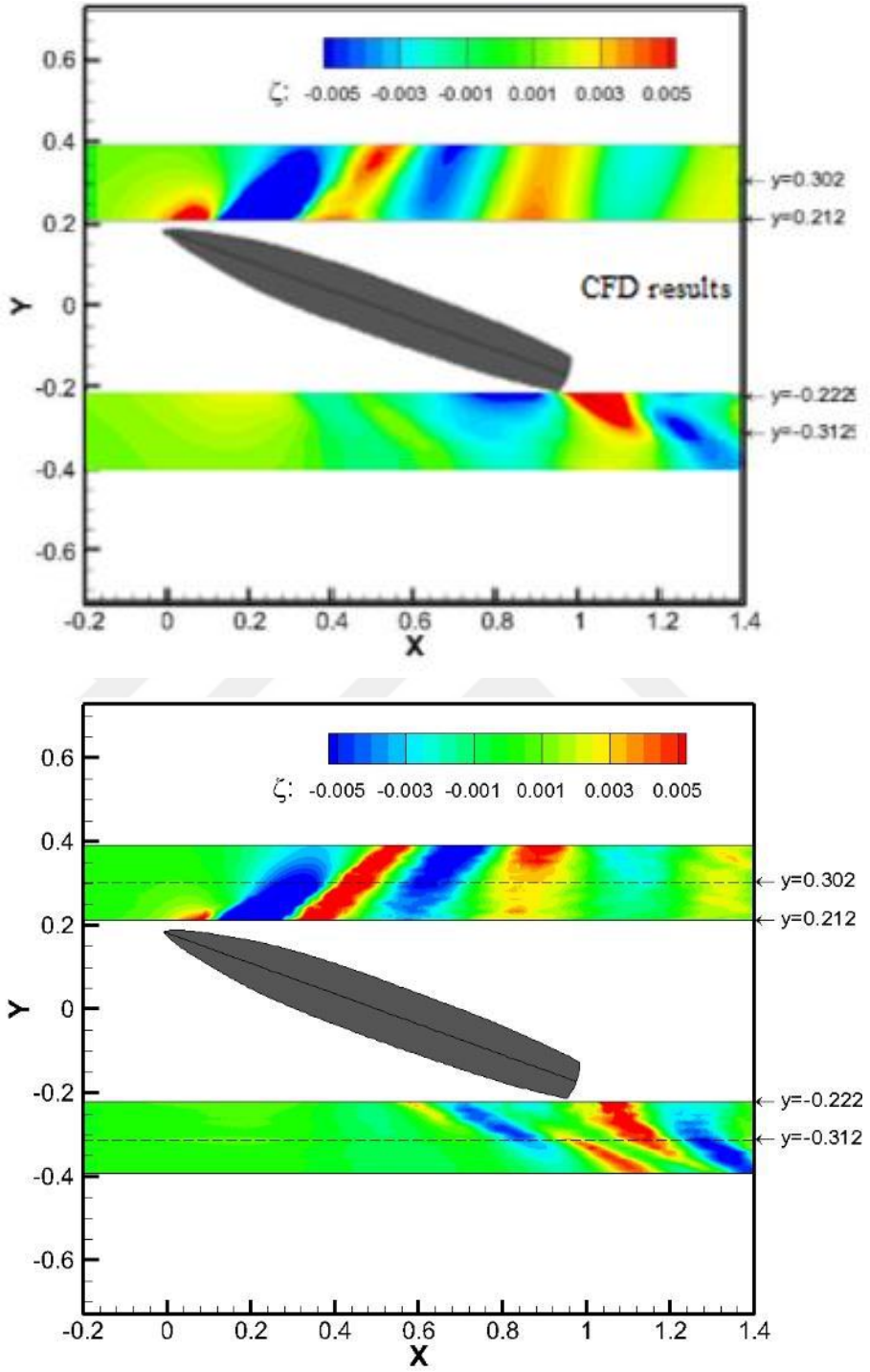

Figure 4.21 : Wave deformations for β=20° condition: CFD-top, EFD-bottom.

The wave contours on the leeward side are agreeable with the EFD data. However, windward side has some differences. Wave contours, which are calculated numerically, on the windward side are shorter and more spread.

To make a more detailed investigation, a particular section is taken from the free surface at y/L=0.302 for 20° drift angle case. The location of this particular section can be seen in Figure 4.21. The wave profile on this section is plotted and compared with the EFD validation data (Figure 4.22). The *x*-axes and *y*-axes of the wave profile figures are nondimensional *x*-position and nondimensional wave elevation, respectively.

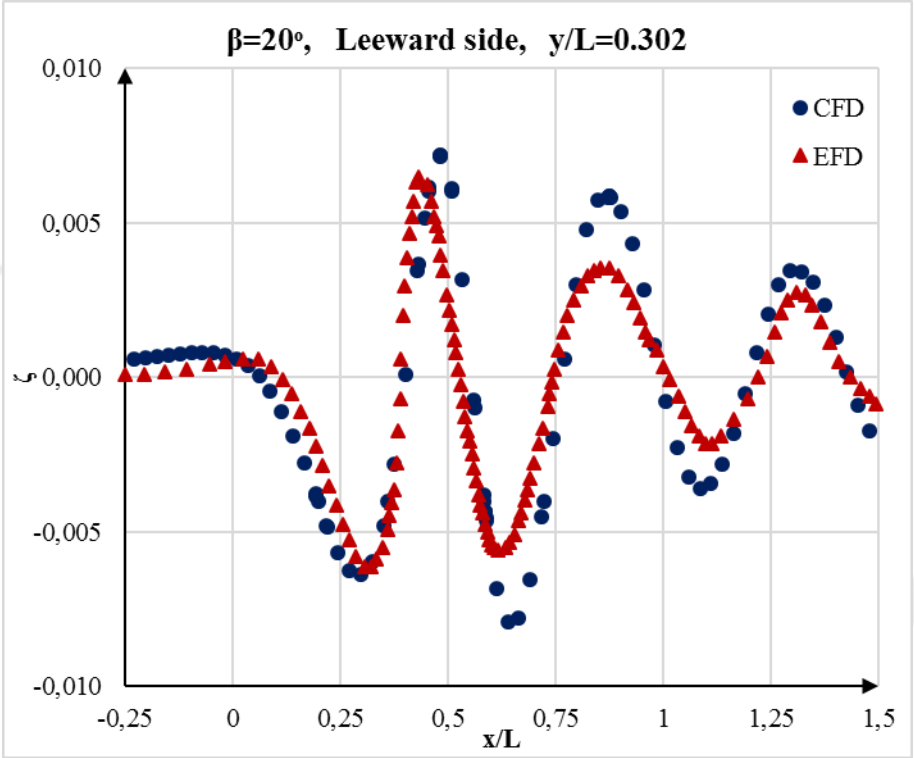

Figure 4.22 : CFD and EFD wave profiles at y/L=0.302 for β=20°.

The general characteristics of numerical results show agreement with the EFD data. Free surface tends to rise around the midship. A wave trough around the first quarter and the last quarter of the ship is observed in both figures. Three wave crests can also be noticed around the x/L=0.6, x/L=0.85 and x/L=1.30 positions.

Figure 4.23 illustrates the flow separation around sonar dome with vorticity magnitude scalar.

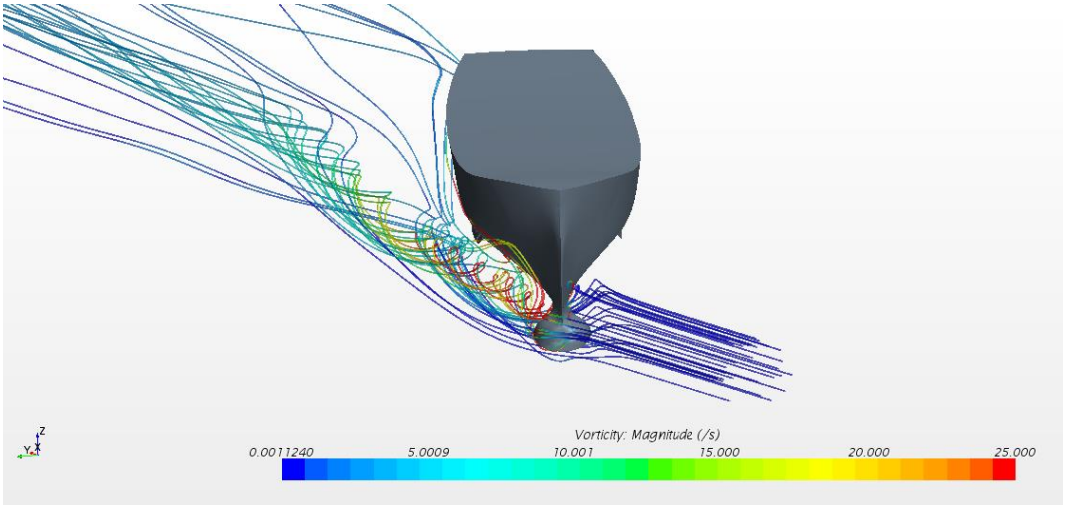

Figure 4.23 : The flow separation around sonardome for β=20°.

4.6 Comparison of Viscous and Inviscid Models

The hydrodynamic forces and moments calculated both for viscous and inviscid flows are shown in Table 4.11.

Table 4.11 : Comparison of viscous and inviscid flows.

Type	Static drift	X'	Y'	N'	ε_X %	ε_Y %	ε_N %
Viscous	β=0°	0.01801	0.00000	0.00000	12.56%	-	-
Inviscid	β=0°	0.00736	0.00000	0.00000	53.98%	-	-
Viscous	β=10°	0.02050	0.06002	0.02295	9.03%	10.54%	12.41%
Inviscid	β=10°	0.00972	0.05929	0.01983	48.31%	9.19%	24.31%
Viscous	β=20°	0.03238	0.14280	0.04076	17.73%	0.59%	26.29%
Inviscid	β=20°	0.02425	0.13586	0.04044	11.81%	5.42%	26.87%

The wave deformations for β=0° and β=20° are given in the following figures (Figure 4.24, Figure 4.25).

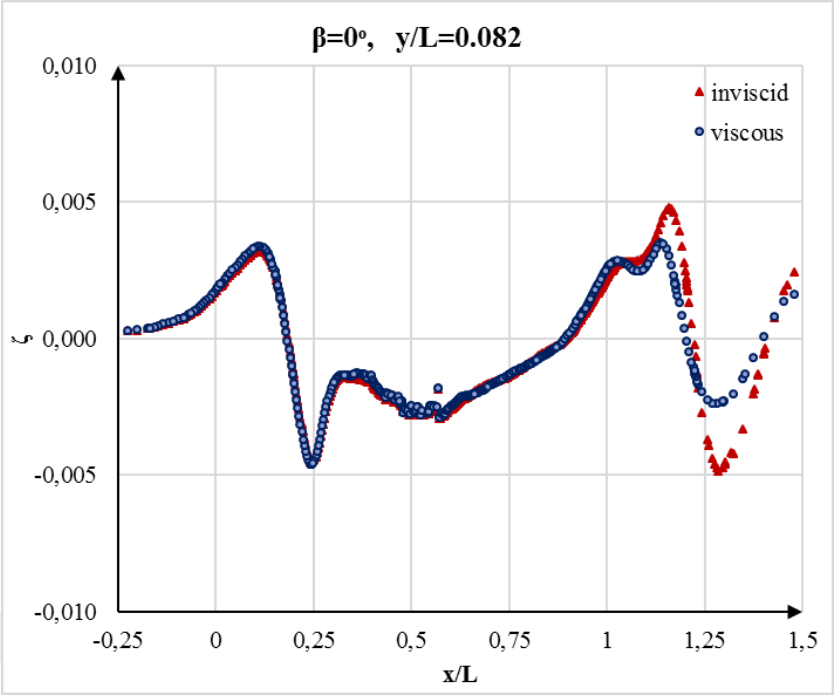

Figure 4.24 : Viscous and inviscid wave profiles at y/L=0.082 for β=0°.

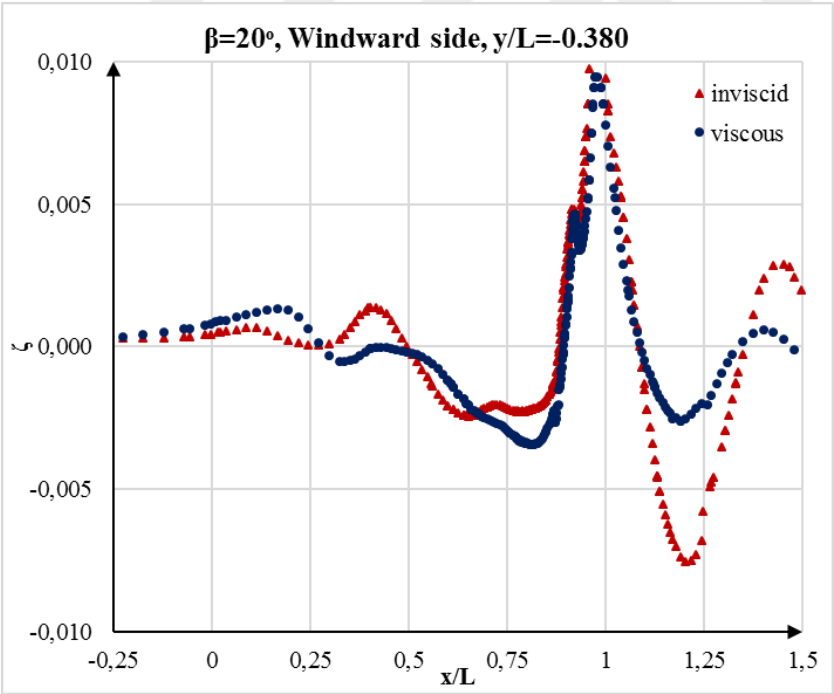

Figure 4.25 : Viscous and inviscid wave profiles at y/L=-0.380 for β=20°.

4.7 Hydrodynamic Derivatives

The forces and moments calculated from static PMM simulations are used to determine the hydrodynamic derivatives.

Table 4.12 : Hydrodynamic derivatives (drift and rudder).

Derivative	Numerical results	Derivative	Numerical results	Derivative	Numerical results
Xδ'	-0.0320	Yδ'	0.2975	Nδ'	0.1416
Xδδ'	0.3548	Yδδ'	-0.2379	Nδδδ'	-0.0303
Xvδ'	-1.1106	Yδδδ'	-0.0928	Nδu'	4.9011
Xδδu'	10.0370	Yδv'	3.3048	Nδδδu'	34.9550
		Yδvv'	-12.2940	Nδvv'	0.1985
		Yvδδ'	-6.7551	Nvδδ'	13.9600
		Yδu'	-3.7854		
		Yδδδu'	-12.5000		

Table 4.13 : Hydrodynamic derivatives (static drift).

Derivative	Numerical results	Yoon (2009)	% ε_R
X*'	-0.0185	-0.0170	8.82
X_{vv}'	-0.1688	-0.1528	10.47
Y_v'	-0.3970	-0.2961	34.08
Y_{vvv}'	-2.0947	-1.9456	7.66
N_v'	-0.1395	-0.1667	16.32
N_{vvv}'	-0.0777	-0.4355	82.16

Table 4.14 shows the empirical hydrodynamic derivatives (Yilmaz, 2008) in comparison with EFD validation data (Yoon, 2009) and numerical results.

Table 4.14 : Empirical hydrodynamic derivatives.

Derivative	Numerical results	EFD	Norrbin	Clarke	Inoue	Wagner Smitt	Ankudinov
Yv'	-0.3970	-0.2961	-0.0102	-0.0063	-0.0102	-0.0094	-0.0098
Yr'	-	-0.0485	0.0026	0.0027	0.0029	0.0019	0.0000
Nv'	-0.1395	-0.1667	-0.0036	-0.0036	-0.0038	-0.0037	-0.0043
Nr'	-	-0.0485	-0.0022	0.0092	-0.0571	-0.0012	-0.0020

4.8 Turning Maneuver Simulation

The turning maneuver simulation results of DTMB model 5415 will be given in this section. A computer program called as DYNEQNOMS has been developed within this thesis to solve the ship-maneuvering motion equations simultaneously according to the Abkowitz's mathematical model. The hydrodynamic derivatives calculated from the

numerical analyses are put into the ship maneuvering simulator to simulate the turning maneuver (Figure 4.26). Motion equations are written in matrix form and solved via Gauss-Jordan Elimination method. The Euler method is used to calculate each velocity components for the next time step. The time step is chosen as $2x10^{-2}$.

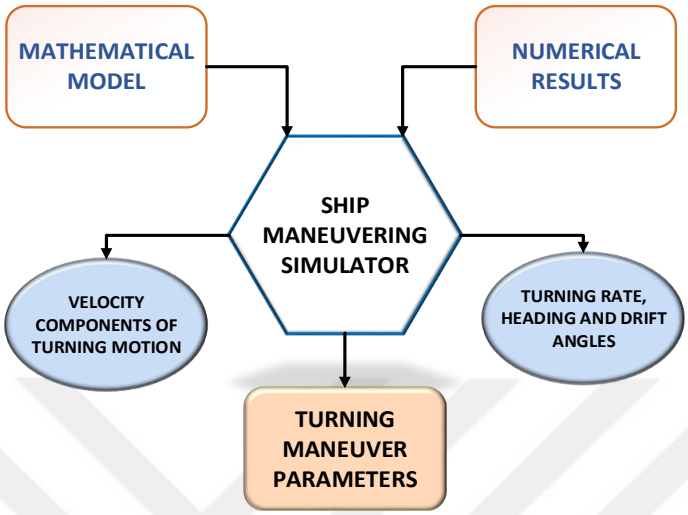

Figure 4.26 : Ship maneuvering simulator diagram.

The computer program gives the turning maneuver parameters, e.g., velocity components of turning motion, turning rate, heading angle and advance, as outputs. Besides, the straight-line stability of DTMB 5512 is investigated.

Table 4.15 : Straight-line stability terms.

Straight-line stability terms	Quantity
m'	0.0058
xg'	0.5052
Yv'	-0.3970
Nv'	-0.1395
Yr'	-0.1970
Nr'	-0.0704
ρ	997.5610
L	3.0480

Table 4.15 gives the terms which are used in stability index formula described in Chapter 2. The straight-line stability index is calculated as C=0.00082. According to mathematical model, positive stability index indicates that the ship has straight-line stability.

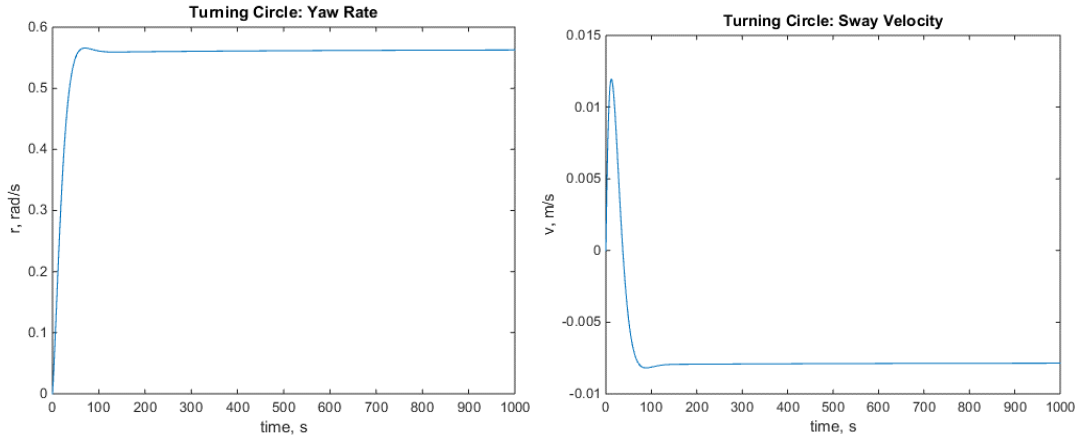

Figure 4.27 : Turning maneuver: yaw rate (left) and sway velocity (right).

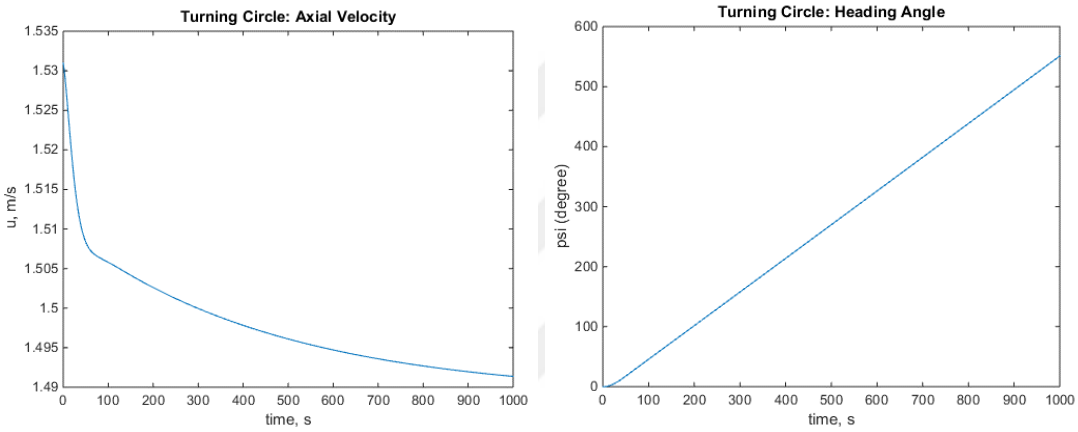

Figure 4.28 : Turning maneuver: axial velocity (left) and heading angle (right).

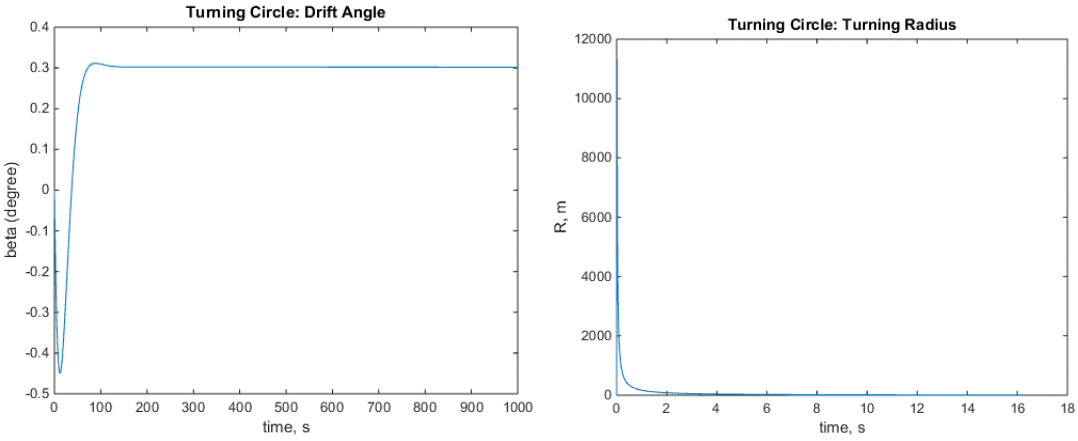

Figure 4.29 : Turning maneuver: drift angle (left) and turning radius (right).

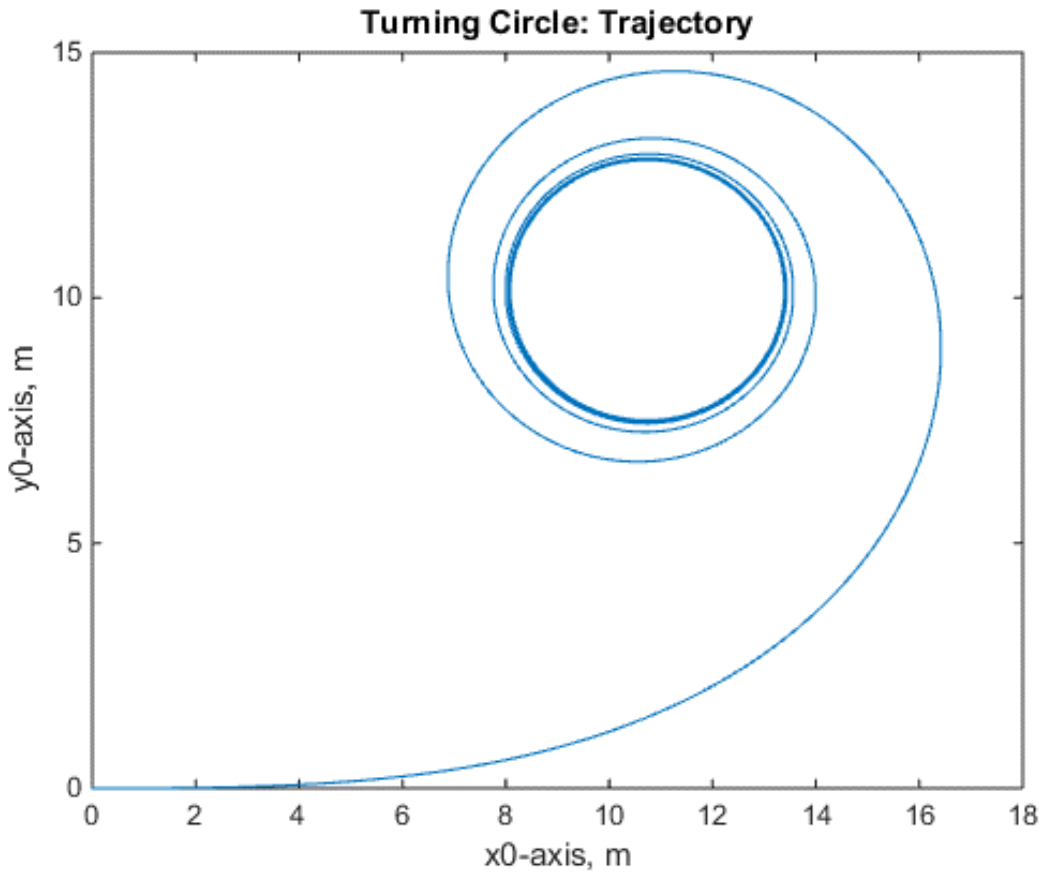

Figure 4.30 : Turning maneuver: trajectory.

The steady turning diameter is compared with the linear model and several empirical formulations (Table 4.16). The tactical diameter is compared with the experimental and numerical validation data (Table 4.17).

Table 4.16 : Steady turning diameter.

	Steady turning radius (m)	Steady turning diameter (m)
Linear model	3.8025	7.6051
Thieme	0.8039	1.6078
Schoenherr	7.9681	15.936
Lyster & Knight	7.5034	15.007
CFD	2.6506	5.3012

The nonlinear model estimates the steady turning diameter lower than linear model. The selected empirical formulas were proposed for cargo ships and not suitable for warships.

Table 4.17 shows that the numerical results are compitable with the available numerical and experimental data (Stern et al., 2011).

Table 4.17 : Tactical diameter.

	Tactical diameter
CFD	$4.79L_{PP}$
FORCE PMM	$4.05L_{PP}$
MARIN - Free sailing	$4.55L_{PP}$
MARIN - Sursim	$2.6L_{PP}$
IOWA RANS Cst RPM	$4.6L_{PP}$

5. CONCLUSION AND DISCUSSION

The computational results show good agreement with the available EFD data. The URANS method is found to be suitable for the presented ship-maneuvering problem. The grid independence study shows that the finer grid gives the better results. Although, k-ω *SST* gives better results in the calculation of sway force at low drift angles, k-ε turbulence model gives more accurate results than k-ω *SST* considering the overall table. Therefore, k-ε turbulence model is used for the analyses. Wave profiles along the ship model are compatible with the experimental results. To investigate the effect of viscosity, several cases have been simulated both with URANS and Euler methods and the results are compared with each other and the available experimental data. As expected Eulerian approach is insufficient for capturing the wave deformations in the wake zone and for positive drift angles it may also be insufficient along the hull. Besides, the hydrodynamic forces are computed with unexceptable errors when compared with EFD data. Therefore the computations are performed for viscous flow.

The hydrodynamic derivatives are calculated in a satisfactory manner for practical applications. The derivatives arising from acceleration and angular velocity are taken from the experimental data (Yoon, 2009). The rudder terms are also determined numerically. Turning maneuver of DTMB model 5512 is simulated by custom developed ship-maneuvering simulator called as DYNEQNOMS which is developed in the scope of this study. The turning maneuver parameters are compared with empirical formulas and available validation data and the results are promising.

In the future studies, the dynamic PMM tests will be simulated with URANS method and maneuvering coefficients will be calculated including acceleration and angular velocity terms. The heel effect on the turning maneuver will be taken into account. The computational grid quality will be increased. Besides turning maneuver, the other definite maneuvers, e.g., the zig-zag, spiral and pull-out maneuvers, will also be simulated with the ship-maneuvering simulator. The maneuvering performance of multihull vessels such as; catamaran, trimaran, will be investigated.

REFERENCES

Abkowitz, M. A. (1964). Lectures on Ship Hydrodynamics – Steering and Maneuvering. Hy-5. Lyngby, Denmark: Hydro & Aerodynamic Laboratory.

Ankudinov, V. (1987). Ship Maneuvrability Assessment in Ship Design: Simulation Concept. In . London.

Artyszuk, J. (2003). A Look into Motion Equations of the ESSO OSAKA Manoeuvring. In , 50:297–315.

Bal, Sakir. (2008a). Performance Prediction of Surface Piercing Bodies in Numerical Towing Tank. *International Journal of Offshore and Polar Engineering* 18 (2): 106–11.

Bal, Sakir. (2008b). Prediction of Wave Pattern and Wave Resistance of Surface Piercing Bodies by a Boundary Element Method. *International Journal for Numerical Methods in Fluids* 56 (3): 305–29. doi:10.1002/fld.1527.

Bertram, Volker. (2012). *Practical Ship Hydrodynamics*. 2. ed. Oxford: Elsevier.

Bhattacharyya, Rameswar. (1978). *Dynamics of Marine Vehicles*. Ocean Engineering. New York: Wiley.

Bhushan, S., T. Xing, P. Carrica, and F. Stern. (2007). Model- and Full-Scale URANS/DES Simulations for Athena R/V Resistance, Powering, and Motionos. *Numerical Ship Hydrodynamics Conference* II: 122–42.

Bhushan, S., Hyunse Yoon, Frederick Stern, E. Guilmineau, M. Visonneau, S. Toxopeus, C. Simonsen, S. Aram, S-E Kim, and G. Grigoropoulos. (2015). CFD VALIDATION FOR SURFACE COMBATANT 5415 AT STRAIGHT-AHEAD AND 20 DEGREE STATIC DRIFT CONDITIONS. Technical Report 493. IIHR-Hydroscience & Engineering: University of Iowa.

Broglia, R., R. Muscari, and A. Di Mascio. (2006). Numerical Analysis of Blockage Effects in PMM Tests. In . Rome, Italy.

Carrica, P. M., and F. Stern. (2008). DES Simulations of KVLCC1 in Turn and Zigzag Manoeuvring with Moving Propeller and Rudder. In . Copenhagen.

CD-adapco. (2014). STAR CCM+ 9.04 User Guide.

Clarke, D., P. Gedling, and G. Hine. (1983). The Application of Manoeuvring Criteria in Hull Design Using Linear Theory. *Transactions of RINA*, 45–68.

Di Mascio, A., and R. Broglia. (2003). Unsteady RANS Calculations of the Flow around a Moving Ship Hull. In . Busan, Korea.

DMI. (2000). PMM Tests with a Model of a Frigate. Experimental Fluid Dynamics 1. Denmark: Danish Maritime Institute.

Dogrul, Ali. (2015). EXPERIMENTAL AND NUMERICAL INVESTIGATION OF SHIP RESISTANCE AND FREE SURFACE DEFORMATIONS (in Turkish). PhD Thesis, Yildiz Technical University.

Dogrul, Ali, and Celik, Fahri. (2016). AN EXPERIMENTAL AND NUMERICAL INVESTIGATION OF RESISTANCE COMPONENTS AND FREE SURFACE DEFORMATIONS FOR A MEDIUM SPEED DISPLACEMENT VESSEL. *Brodogradnja*, 47–65. doi:10.21278/brod67204.

Faltinsen, Odd. (2006). *Hydrodynamics of High-Speed Marine Vehicles.* Cambridge: Cambridge University Press. http://www.myilibrary.com?id=91756.

Ferziger, Joel H., and Milovan Perić. (2002). *Computational Methods for Fluid Dynamics*. 3., rev. ed. Berlin: Springer.

Fonfach, Jose Miguel Ahumada. (2010). Numerical Study of the Hydrodynamic Interaction between Ships in Viscous and Inviscid Flow. PhD Thesis, Universidade de Lisboa.

Fossen, Thor I. (1994). *Guidance and Control of Ocean Vehicles*. Chichester ; New York: Wiley.

Gertler, M. (1966). Cooperative Rotating-Arm and Straight Line Experiments with ITTC Standard Model (Mariner Type Ship). 2221. David Taylor Model Basin.

Gertler, Morton. (1967). THE DTMB PLANAR-MOTION-MECHANISM SYSTEM. TEST AND EVALUATION REPORT AD659053. Washington, DC: Naval Ship Research and Development Center.

Hirt, C.W, and B.D Nichols. (1981). Volume of Fluid (VOF) Method for the Dynamics of Free Boundaries. *Journal of Computational Physics* 39 (1): 201–25. doi:10.1016/0021-9991(81)90145-5.

Hooft, J.P. (1994). The Cross-Flow Drag on a Manoeuvring Ship. *Ocean Engineering* 21 (3): 329–42. doi:10.1016/0029-8018(94)90004-3.

IMO. (1993). INTERIM STANDARTS FOR SHIP MANOEUVRABILITY. Resolution A.751(18). IMO.

Inoue, S., M. Hirano, and K. Kijima. (1981). Hydrodynamic Derivatives on Ship Manoeuvring. *International Shipbuilding Progress* 28 (321): 112–25.

ITTC. (2002). Captive Model Test Procedure. Recommended Procedures 7.5-02-06-02. ITTC MANEUVERING COMMITTEE.

ITTC. (2014). Free Running Model Tests. Recommended Procedures 7.5-02-06-01. ITTC MANEUVERING COMMITTEE.

Jones, W.P, and B.E Launder. (1972). The Prediction of Laminarization with a Two-Equation Model of Turbulence. *International Journal of Heat and Mass Transfer* 15 (2): 301–14. doi:10.1016/0017-9310(72)90076-2.

Kijima, K., and Y. Nakiri. (2003). On the Practical Predic-Tion Method for Ship Manoeuvring Characteristics. In , 105:21–31. Trans West Japan Soc Naval Arch.

Kijima, K., Y. Nakiri, Y. Tsusui, and M. Matsunaga. (1990). Prediction Method of Ship Manoeuvrability in Deep and Shallow Waters. In . Tokyo, Japan.

Kijima, K., S. Tanaka, Y. Furukawa, and T. Hori. (1993). On a Prediction Method of Ship Manoeuvring Characteristics. In , 1:285–94.

Kim, Hyuncheol, Hiromichi Akimoto, and Hafizul Islam. (2015). Estimation of the Hydrodynamic Derivatives by RaNS Simulation of Planar Motion Mechanism Test. *Ocean Engineering* 108 (November): 129–39. doi:10.1016/j.oceaneng.2015.08.010.

Kim, S. E., and S. H. Rhee. (2002). High-Incidence and Dynamic Pitch-Up Maneuvering Characteristics of a Prolate Spheroid - CFD Validation. In . Fukuoka, Japan.

Kim, W. J., S. H. Van, and D.-H. Kim. (2001). Measurement of Flows Around Commercial Ship Models. *Experiments in Fluids* 31 (5): 567–78.

Larsson, L., F. Stern, and Volker Bertram. (2003). Benchmarking of Computational Fluid Dynamics for Ship Flows: The Gothenburg 2000 Workshop. *Journal of Ship Research* 47 (1): 63–81.

Lewis, Edward V., ed. (1989). *Motions in Waves and Controllability*. 2. revision, 1. print. Principles of Naval Architecture, Edward V. Lewis, ed. ; 3. Jersey City, NJ: Society of Naval Architects and Marine Engineers.

Longo, J., and F. Stern. (2005). Uncertainty Assessment for Towing Tank Tests with Example for Surface Combatant DTMB Model 5415. *Journal of Ship Research* 49 (1): 55–68.

Martinussen, K., and E. Ringen. (2008). Simulation of KVLCC1 and KVLCC2 Manoeuvring Motion. In . Copenhagen.

Moreira, L., and C. Guedes Soares. (2003). Dynamic Model of Manoeuvrability Using Recursive Neural Networks. *Ocean Engineering* 30 (13): 1669–97. doi:10.1016/S0029-8018(02)00147-6.

SNAME. (1952). Nomenclature for Treating the Motion of a Submerged Body through a Fluid. (1952). Technical and Research Bulletin 1-5. SNAME.

Norrbin, N. H. (1971). Theory and Observations on the Use of a Mathematical Model for Ship Manoeuvring in Deep and Confined Waters. *SWEDISH STATE SHIPBUILDING EXPERIMENTAL TANK*, no. 68.

Oltmann, P. (2000). 25 Years Computerized Planar Motion Carriage at HSVA – A Resume. In . Hamburg.

Sabuncu, Tarik. (1985). *GEMİ MANEVRALARI VE KONTROLÜ*. İTÜ Gemi İnşaatı ve Deniz Bilimleri Fakültesi Ofset Baskı Atölyesi.

Sakamoto, Nobuaki. (2009). URANS AND DES SIMULATIONS OF STATIC AND DYNAMIC MANEUVERING FOR SURFACE COMBATANT. PhD Thesis, University of Iowa.

SIMMAN 2014. (2014). GEOMETRY AND CONDITIONS OF US NAVY COMBATANT. *simman2014.dk*. http://simman2014.dk/ship-data/us-navy-combatant/geometry-and-conditions-us-navy-combatant/.

Simonsen, C. D., F. Stern, and K. Agdrup. (2006). CFD with PMM Test Validation for Manoeuvring VLCC2 Tanker in Deep and Shallow Water. In . Terschelling, Netherlands, M-4-1.

Simonsen, Claus D., Janne F. Otzen, Christian Klimt, Nikolaj L. (FORCE Technology Larsen Denmark), and Frederick (IIHR Stern University of Iowa, USA). (2012). Maneuvering Predictions in the Early Design Phase Using CFD Generated PMM Data. In . Gothenburg, Sweden.

Simonsen, Claus D., and Fred Stern. (2003). Verification and Validation of RANS Maneuvering Simulation of Esso Osaka: Effects of Drift and Rudder Angle on Forces and Moments. *Computers & Fluids* 32 (10): 1325–56. doi:10.1016/S0045-7930(03)00002-1.

Smitt, W. L. (1970). Steering and Manoeuvring Full-Scale and Model Tests (Part 1). *Europian Shipbuilding* 19 (6).

Stern, F., K. Agdrup, S. Y. Kim, A. C. Hochbaum, K. P. Rhee, F. Quadvlieg, P. Perdon, T. Hino, R. Broglia, and J. Gorski. (2011). Experience from SIMMAN 2008—The First Workshop on Verification and Validation of Ship Maneuvering Simulation Methods. *Journal of Ship Research*, no. 55 (June): 135–47.

Stern, Fred, Robert V. Wilson, Hugh W. Coleman, and Eric G. Paterson. (2001). Comprehensive Approach to Verification and Validation of CFD Simulations—Part 1: Methodology and Procedures. *Journal of Fluids Engineering* 123 (4): 793. doi:10.1115/1.1412235.

Strom-Tejsen, J., and M. S. Chislett. (1966). A Model Testing Technique and Method of Analysis for the Prediction of Steering and Manoeuvering Qualities of Surface Vessels. Hy-7. Lyngby, Denmark: Hydro & Aerodynamic Laboratory.

Tahara, Y., J. Longo, and F. Stern. (2002). Comparison of CFD and EFD for the Series 60 CB=0.6 in Steady Drift Motion. *Journal of Marine Science and Technology* 7 (1): 17–30.

Toxopeus, S. (2006). Calculation of Hydrodynamic Manoeuvring Coefficients Using Visous- Flow Calculations. In . Ischia, Italy.

Toxopeus, S. L., and S. W. Lee. (2008). Comparison of Manoeuvring Simulation Programs for SIMMAN Test Cases. In . Copenhagen.

Ucer, Erdem. (2011). Examination of the Stability of Trawlers in Beam Seas by Using Safe Basins. *Ocean Engineering* 38 (17-18): 1908–15. doi:10.1016/j.oceaneng.2011.09.027.

Uslu, Yasin, and Bal, Sakir. (2008). Numerical Prediction of Wave Drag of 2-D and 3-D Bodies under or on a Free Surface. *Turkish Journal of Engineering and Environmental Science* 32: 177–88.

Viviani, M., R. Depascale, L. Sebastiani, C. P. Bonvino, R. Dattola, and M. Soave. (2003). Alternative Method for the Identification of Hydrodynamic Coefficients from Standard Manoeuvres. In , RC – 5.

Yasukawa, H., and Y. Yoshimura. (2015). Introduction of MMG Standard Method for Ship Maneuvering Predictions. *Journal of Marine Science and Technology* 20 (1): 37–52. doi:10.1007/s00773-014-0293-y.

Yilmaz, Tamer, ed. (2008). *Gemi Mühendisliği El Kitabı*. Gemi Mühendisleri Odası.

Yoon, Hyeon Kyu, and Key Pyo Rhee. (2003). Identification of Hydrodynamic Coefficients in Ship Maneuvering Equations of Motion by Estimation-Before-Modeling Technique. *Ocean Engineering* 30 (18): 2379–2404. doi:10.1016/S0029-8018(03)00106-9.

Yoon, Hyunse. (2009). Phase-Averaged Stereo-PIV Flow Field and Force/ Moment/motion Measurements for Surface Combatant in PMM Maneuvers. PhD Thesis, University of Iowa.

Yoon, Hyunse, Claus D. Simonsen, Lanfranco Benedetti, Joseph Longo, Yasuyuki Toda, and Frederick Stern. (2015). Benchmark CFD Validation Data for Surface Combatant 5415 in PMM Maneuvers – Part I: Force/moment/motion Measurements. *Ocean Engineering* 109 (November): 705–34. doi:10.1016/j.oceaneng.2015.04.087.

Yoshimura, Yasuo. (2005). Mathematical Model for Manoeuvring Ship Motion (MMG Model). In . Tokyo.

Zikanov, Oleg. (2010). *Essential Computational Fluid Dynamics*. Hoboken, NJ: Wiley.

APPENDICES

APPENDIX A: Turbulent kinetic energy and vorticity magnitude for β=0°
APPENDIX B: Turbulent kinetic energy and vorticity magnitude for β=20°

APPENDIX A

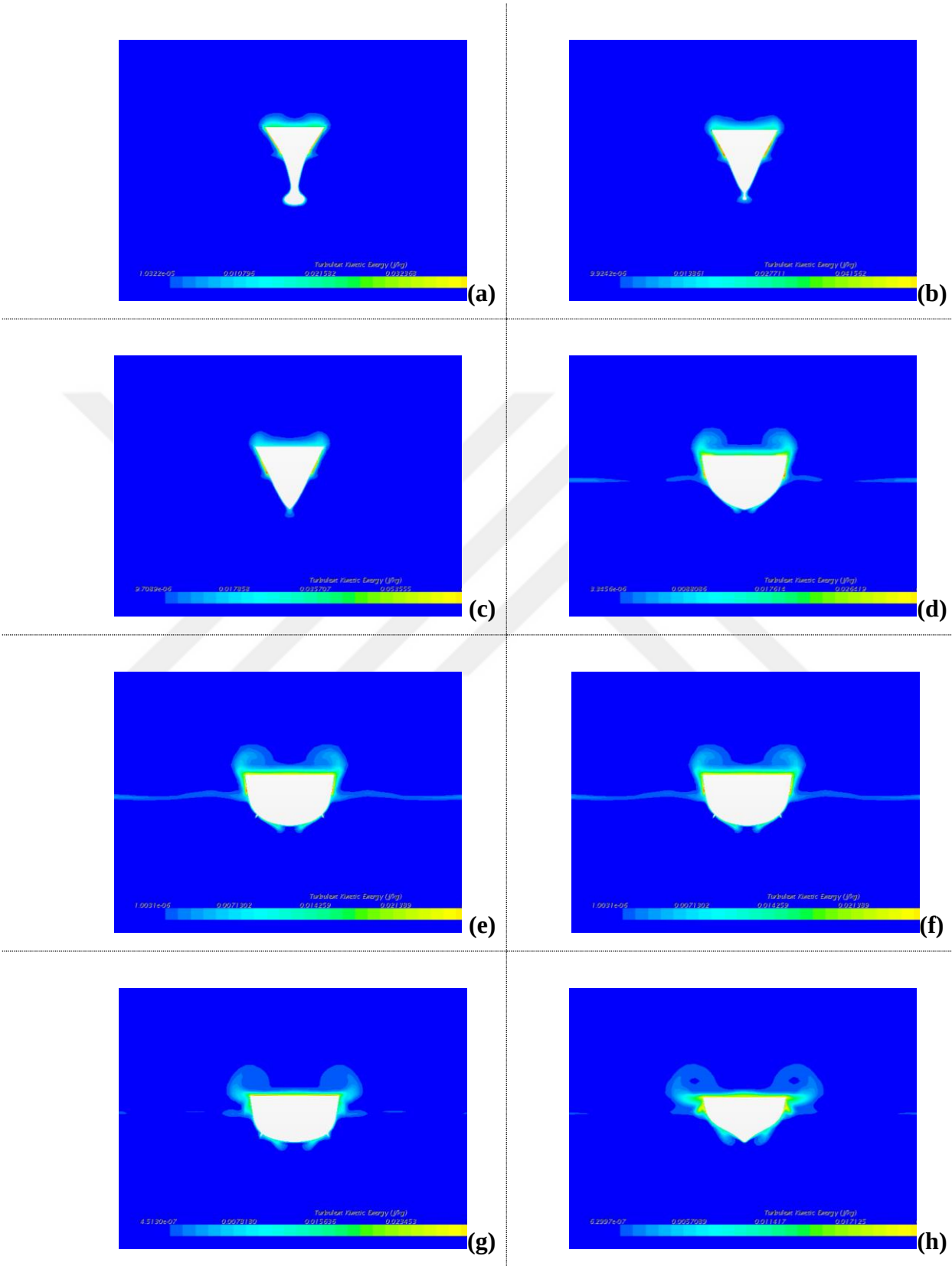

Figure A.1 : Turbulent kinetic energy ($\beta=0°$): (a) x/L=0.06. (b) x/L=0.1. (c) x/L=0.12. (d) x/L=0.2. (e) x/L=0.3. (f) x/L=0.4. (g) x/L=0.6. (h) x/L=0.8.

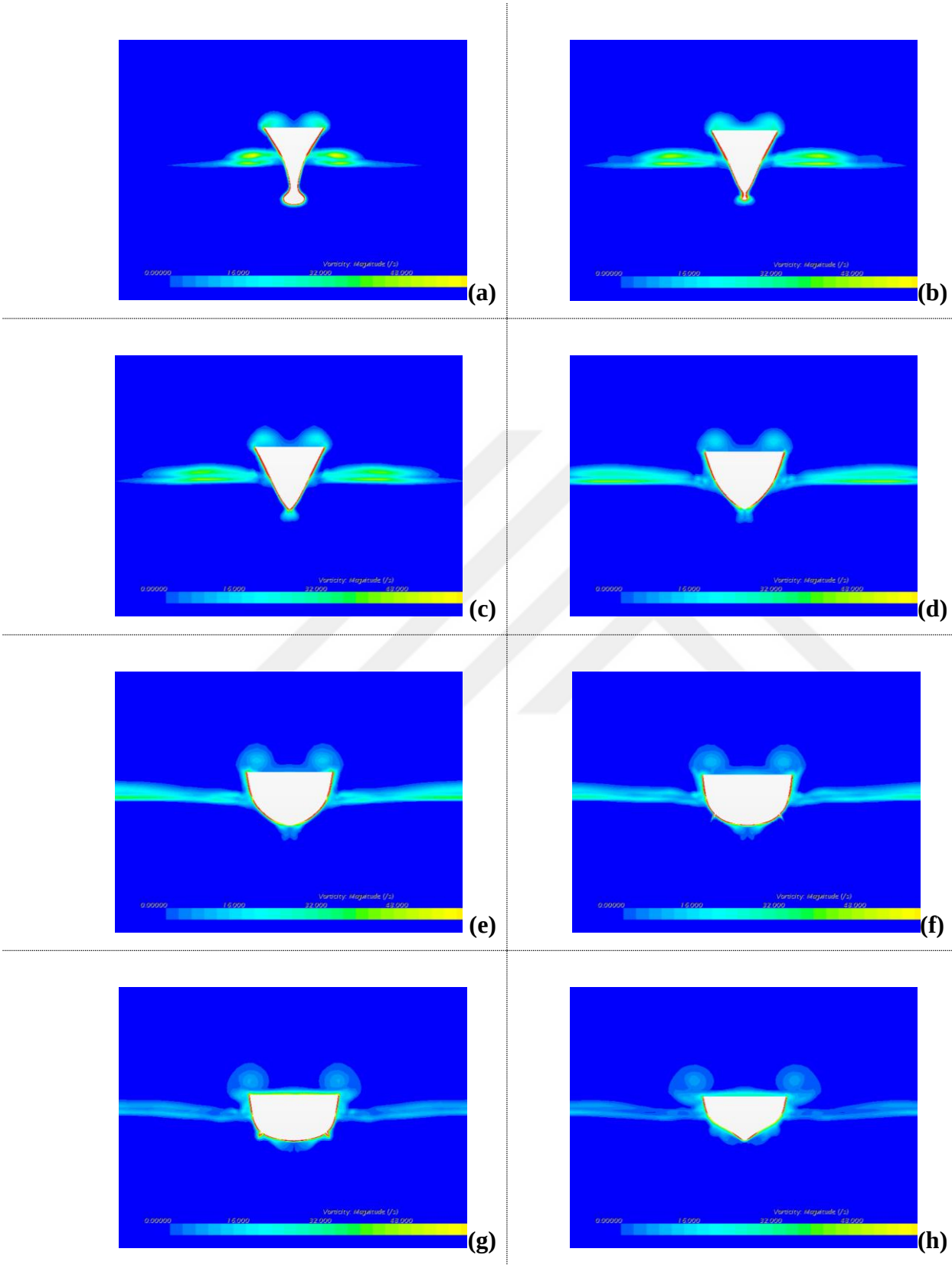

Figure A.2 : Vorticity magnitude ($\beta=0°$): (a) x/L=0.06. (b) x/L=0.1. (c) x/L=0.12. (d) x/L=0.2. (e) x/L=0.3. (f) x/L=0.4. (g) x/L=0.6. (h) x/L=0.8.

APPENDIX B

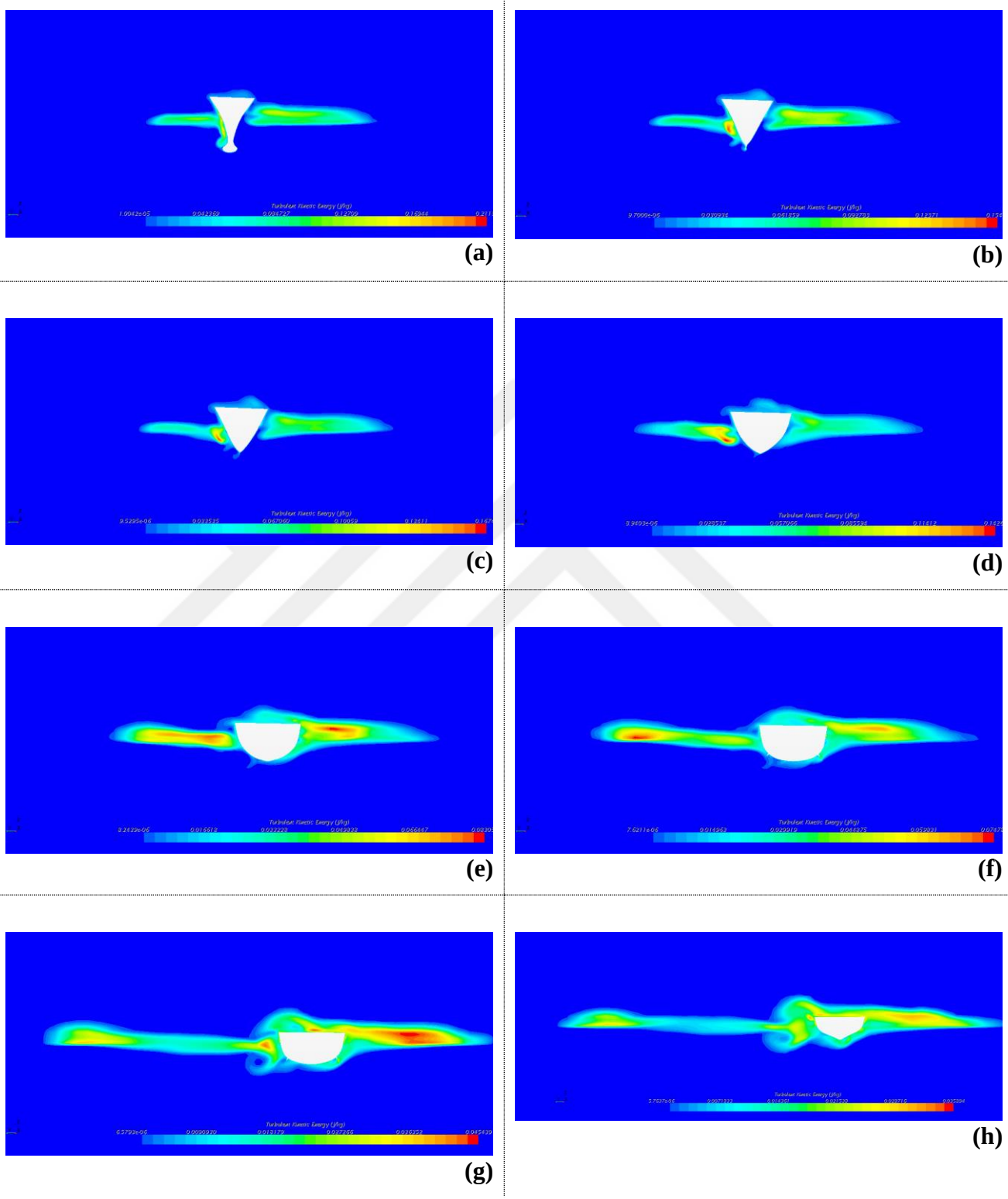

Figure B.1 : Turbulent kinetic energy (β=20°): (a) x/L=0.06. (b) x/L=0.1. (c) x/L=0.12. (d) x/L=0.2. (e) x/L=0.3. (f) x/L=0.4. (g) x/L=0.6. (h) x/L=0.8.

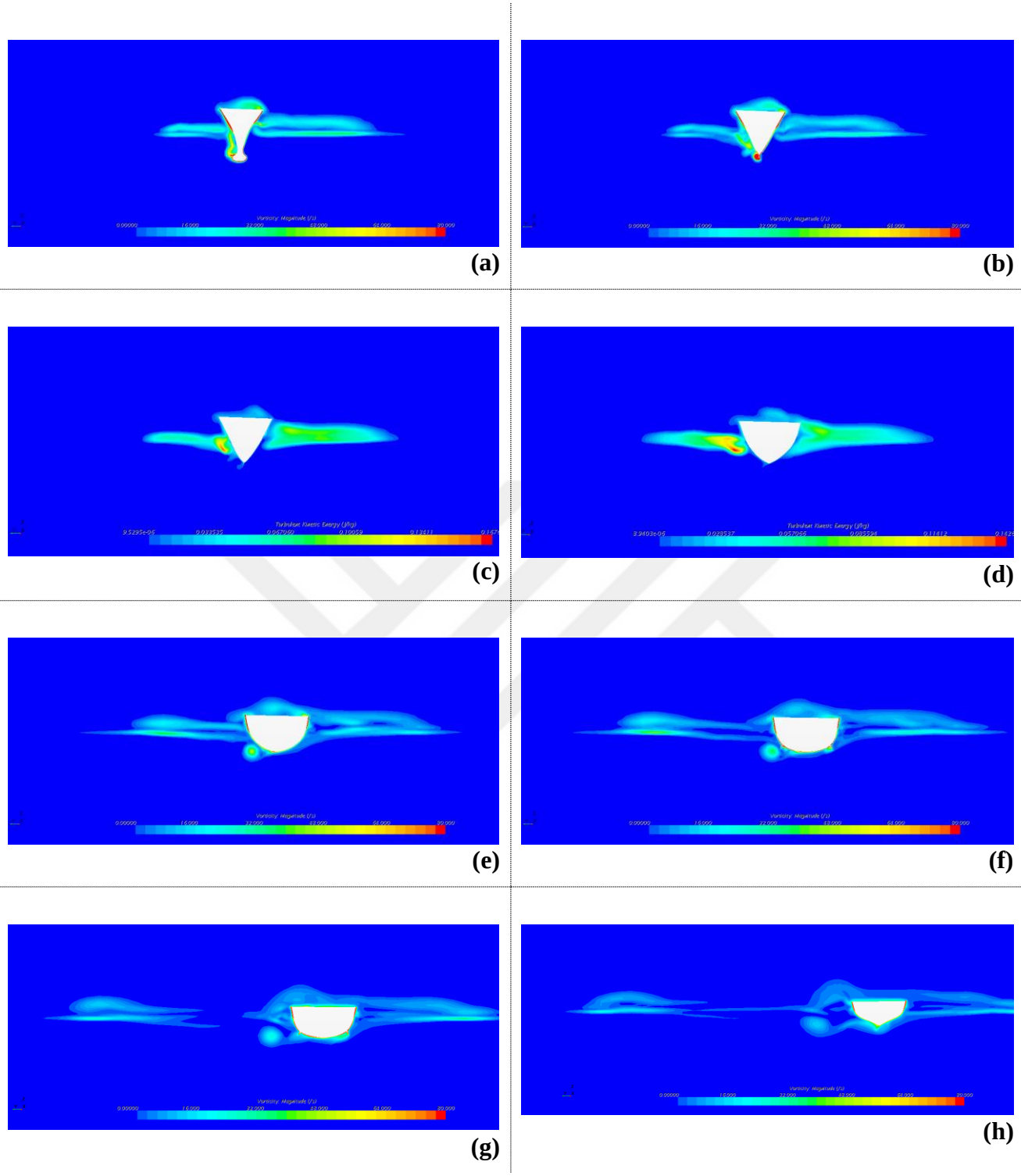

Figure B.2 : Vorticity magnitude ($\beta=20°$): (a) x/L=0.06. (b) x/L=0.1. (c) x/L=0.12. (d) x/L=0.2. (e) x/L=0.3. (f) x/L=0.4. (g) x/L=0.6. (h) x/L=0.8.

CURRICULUM VITAE

Name Surname **:** Süleyman DUMAN

Place and Date of Birth **:** Hatay / 17.06.1991

E-Mail **:** gimsuleymanduman@gmail.com, sduman@yildiz.edu.tr

EDUCATION **:**

- **B.Sc.** **:** 2014, YTU, Naval Architecture and Maritime Faculty, Department of Naval Architecture and Marine Engineering

PROFESSIONAL EXPERIENCE AND REWARDS:

- 2015-2016 Research Assistant at the Department of Naval Architecture and Marine Engineering at YTU.
- 2014 Honors Degree in Naval Arch. and Marine Eng. (BSc.), YTU.

PUBLICATIONS, PRESENTATIONS AND PATENTS ON THE THESIS:

- Sezen, S., Duman, S., Kaplan, O., Ünsan, Y., and Korkut, E., 2015. Deniz Sektöründe Kullanılan Kompozit Malzemelerin Mekanik Özelliklerinin Belirlenmesi için Basit Bir Deney Düzeneği, *İTÜ GİDB DERGİ*, Vol 3, Pg 41-62.
- Duman, S., Dogrul, A., Kahramanoğlu, E., 2016: On the Uncertainty Analysis of DTMB5415 for Form Factor Prediction. 2nd GMT Conference, Mugla, Turkey.